Crustal Imaging of Prospective Geothermal Basins Using Magnetotellurics: a case study of the Renmark Trough in South Australia

Emily Craven (B.Sc. Honours)
2009

University of Adelaide
North Terrace, SA, 5005
Australia

emily.craven@adelaide.edu.au or
emily.craven@live.com.au

Supervisor: Graham Heinson

Table of Contents

ABSTRACT

The presence of anomalously high geothermal gradients in South Australia has led to increased geothermal exploration and an associated demand for cost effective methods to explore the subsurface of a region before drilling. This case study is aimed at delineating the basement structure of prospective geothermal basins, in particular the Renmark Trough tenement held by Petratherm in South Australia, using magnetotelluric (MT) and geomagnetic depth sounding (GDS) data. The effectiveness of the MT data has been compared to both gravity and seismic data in the area and 1D resistivity models have been used to estimate the temperature gradient range in the area. Broadband and long-period MT data were obtained in 2009 5 km northwest of Renmark, South Australia, along two, two-dimensional profiles perpendicular to the Hamley Fault and across the Renmark Trough. The MT data fit all two-dimensional smooth inversions produced to a root-mean square (rms) misfit of 2.2 or less. The broadband resistivity model shows a higher resistivity basement (40-100 Ωm) below low resistivity (0.3-12 Ωm) sediments in a half graben structure of 4 km depth, apparently shallowing to 3-3.5 km and forming a graben structure 10 km north along the lower resolution long-period profile. Comparison between MT, gravity and seismic data revealed an additional low permeability structure in the MT model between the highly conductive sediments and seismically constrained basement. Magnetotelluric resistivity data identified basement depth at 4km in a seismically complex area where seismic data are unable to image due to the presence of high angled faults. Due to a lack of constraints in the Renmark area, rough temperature gradient calculations have resulted in large ranges for the gradient in the deepest section of the trough, with 75-110 ºC/km for a mainly sand lithology (Cooltong 1 drillhole) or 50-75 ºC/km for a mainly silt lithology (North Renmark 1 drillhole). With additional information from relogging existent well bores and drilling new wells, the temperature calculations could be more tightly constrained.

Keywords: Geothermal energy; magnetotellurics; gravity; seismic; temperature gradient; Renmark Trough; exploration methods.

1. INTRODUCTION

Conventional geothermal energy is produced using hot water from relatively shallow aquifers in volcanic regions (Hillis *et al.* 2004). The lack of evidence for recent magmatism or significant crustal extension in South Australia, and Australia in general, makes such conventional energy production a low possibility (Reid & Hand 2005). In contrast, hot dry rock (HDR) geothermal energy is obtained by circulating water between injection and production wells through hot subsurface rocks. Compared to conventional geothermal systems these rocks are generally deep, impermeable and contain little to no porosity or fluid content (Hillis *et al.* 2004). Hot dry rock geothermal resources worldwide are estimated to total 42-422 x 10^{24} J, a resource that is 100-1000 times larger than the fossil energy resource (Duchane 1994). In Australia, Somerville *et al.*'s (1994) map of estimated temperature at 5 km depth in the Australian crust (measuring 3,291 wellbores) shows that large areas of Australia have temperatures of >250 ºC at 5 km. The largest area recognised by Somerville *et al.* (1994) is under the Great Artesian (Eromanga) Basin, although this is partly due to the density of data from well-constrained hydrocarbon borehole information in the overlying Cooper Basin (Hillis *et al*. 2004).

The majority of previous HDR projects have focused on areas of known high (>55 ºC) geothermal gradients such as European Soultz-sous-Forêts project, France, or Geodynamics' Habanero-1 well in the Cooper Basin (Hillis *et al*. 2004). South Australia has become a focus for HDR geothermal prospectivity due to its exceptionally hot subsurface rocks. Though the data from Somerville *et al.*'s (1994) map is sparse, modelling of the South Australian Heat Flow Anomaly (SAHFA; Figure 1) indicates possibly higher geothermal gradients than those seen in the Cooper Basin (Neumann *et al.* 2000). The average heat flow of the SAHFA is ~ 90 milliW/m^2 (e.g McLaren *et al.* 2003; Cull 1982; Houseman *et al.* 1989) almost twice that of the global average heat flow of Proterozoic continental crust, around 50 milliW/m^2 (Reid & Hand 2005; Morgan 1984; Nyblade & Pollack 1993). The SAHFA's high heat flow is not attributed to crustal volcanism (Reid & Hand 2005). Additionally shear wave velocities underlying eastern South Australia show comparatively cool mantle at around 250 km depths suggesting no significant mantle contribution (Fishwick *et al.* 2005). Neumann *et*

al. (2000) concludes that highly anomalous Uranium and Thorium content in crystalline basement is likely to be the primary source of high crustal heat production.

When exploring for prospective HDR geothermal resources in areas unconstrained by deep boreholes, cost effective strategies require the discovery of rocks in excess of 200 ºC at the shallowest possible depth, in close proximity to the national electricity grid. Prospective geothermal resources require a high heat flow and cover sediments with low thermal-conductivity (Hillis *et al.* 2004). It is now recognised that the best hydraulic link between boreholes is enhanced by a pre-existing natural fracture system (Evans *et al.* 1999). Deep drilling, in such wells as Geodynamics Habanero-1 well in the Cooper basin, has revealed fractures that may provide permeable pathways at several kilometres depth in the crust (Fehler 1989; Shapiro *et al.* 1997). As such several concurrent geological factors are explored for in SA:

1. The presence of thermally anomalous granites is one of the key factors. Granites have a generally anomalous high heat-flow due to a large content of radiogenic Potassium, Uranium and/or Thorium. However, many granites within the SAHFA give rise to a higher heat production rate than most normal granites (Hillis *et al.* 2004). For example, the Mt Painter Inlier has an average heat production rate of 10 $\mu W/m^3$ (Neumann *et al*. 2000), four times greater than that of typical granites (McLennan & Taylor 1996). Radiogenic iron oxides (RIO) also have been known to generate an average heat flow 50 times that of average granites (Housmann *et al.* 1989), but they are smaller in volume and less easy to detect. One need not target the heat-producing basement rocks if the immediately overlying cover rocks are sufficiently hot (Hillis *et al.* 2004).

2. The basic control on near surface geothermal gradient is the balance between the insulating properties of the upper-crust and the heat-flow field (Hillis *et al.* 2004). The SAHFA exhibits surface heat flow in the range 70-130 $milliW/m^2$ (Cull 1982; Houseman *et al.* 1989). Figure 2 shows the relation between depth of burial of the heat source and temperature (Hillis *et al.* 2004). This assumes an average thermal conductivity of 2 W/mK (the typical range being 1.5-2.5

W/mK; Hillis *et al.* 2004) for the cover sediments, a typical mantle heat flow of 25 milliWm^{-2} (Zielhuis & Van der Hilst 1996; Debayle & Kennett 2003), a 5 km thick granite layer at the base of the cover sequence with heat production rate of 9 μW/m^3 and a cover sequence generating 1 μW/m^3 (Hillis *et al.* 2004). The figure suggests that for temperatures >200 ºC the cover rocks must exhibit low thermal conductivity and depths must be at least 3 km (Hillis *et al.* 2004). As such it can be concluded that the thermal conductivity and the presence of cover sediments is as important for heating of geothermal basins as the heat producing rock itself.

With current non-unique geophysical and geothermal modelling techniques, the only way to confirm high geothermal gradients within sedimentary basins is to drill. Currently none of the basic calculations can give an estimate as to the possibility of fluid-filled permeable fractures. Seismic reflection has been used to image basement structures, but survey costs are large and seismic poorly images high angle faults. Other geophysical techniques that have been used (but require drilling) include borehole geophysics and the use of self-potential (SP) to determine fluid recharge and discharge areas (Thiel pers. com. 2009) and seismic imaging using microearthquakes cause by drilling and hydraulic fracturing (Block 1994).

A viable alternative to further constrain modelling and so infer the presence of fluid and drilling success, is to use magnetotellurics (MT) and geomagnetic depth sounding (GDS) to investigate the resistivity structure and depth to basement, which can then be used as a proxy for temperature. Resistivity in sedimentary environments is sensitive to porosity (Archie's Law), fluid salinity, fluid temperature (Nesbitt 1993) and clay content and MT can be used to explore these properties. MT is used to define geometries within the earth and is ideal for defining the geometries of basins. Thermal modelling can be more tightly constrained using MT resistivity. The generally high conductivity of fluids should in theory be detectable at depth using MT and indicate a prospective, and more economic hot wet rock system.

This paper deals with an MT case study of the Renmark Trough in South Australia, a prospective geothermal tenement held by Petratherm LTD. This study deployed two MT lines, one broadband MT line and one long-period MT line (to image deeper into the crust), across the Hamley Fault and the Renmark Trough in order to probe the resistivity structure of the subsurface. Both 1D and 2D inversions were produced and integrated with gravity, magnetic and seismic datasets to further constrain the MT model. A rough framework of thermal modelling was then constructed using the 1D resistivity profile.

2. THE GEOLOGY AND GEOPHYSICS OF THE RENMARK TROUGH

2.1 Geology

The Renmark Trough has a north-easterly trend and deepens from ~2700 m in the south to ~3500 m in the north (Thornton 1974; Figure 1; Figure 3). The trough is approximately 24 km wide and extends to over 100 km in length. The southern end appears to be a half graben delineated on its north-western side by the Hamley Fault. The Hamley Fault extends up into overlying Early Cretaceous sediments with a throw of up to 1500 m (Alley 1995). The northern end is a graben with its eastern boundary created by the north-south trending Chowilla Fault which has a similar throw to the Hamley Fault.

Drilling in the Renmark Trough area (Figure 11b) indicates that underlying the Permian Urana Formation and overlying Adelaidean strata or Kanmantoo Group (Alley & Gravestock 1995), is a sequence of clastics thought to be of Devonian age and a probable extension of the Darling Basin in NSW (Thornton 1974). Comprised of fluvial and fluviolacustrine sediments the total thickness is unknown due to termination of drilling within that sequence (Alley & Gravestock 1995). However, seismic datasets suggest that this Devonian sequence may exceed 1500 m thickness in the north decreasing to ~600 m in the south and possibly extending westwards across the Hamley Fault (Thornton 1974).

Late Palaeozoic sediments encountered in several drill holes are preserved and partly deposited in the structurally controlled infrabasins of the Nadda Basin, which includes the Renmark Trough (Alley 1995; Thornton 1974). The basement of the trough was believed to be Devonian by Thornton (1974), but the basement is also likely to contain Adelaidean strata (Alley 1995). The Late Palaeozoic sediments attain a thickness of 900 m in the Renmark Trough. The Urana formation extends southwards from the trough along erosional valleys in the basement that grade towards the trough (Alley 1995).

Overlaying the Late Palaeozoic sediments is the Early Cretaceous Berri Basin, regarded as a probable extension of the Eromanga Basin. The Early Cretaceous sediments are thickest in the Renmark Trough, up to 600 m in seismic datasets, and comprises the Monash Formation and Renmark Group (Rogers 1995). The Monash Formation unconformably overlies Late Palaeozoic Urana Formation (O'Brien 1986) and is unconfomably overlain by the Late Paleocene to Early Oligocene Renmark Group. The sediments indicate a sequence of marine transgression, uplift, freshwater sedimentation and further uplift in the Albian which ended sedimentation. Erosion later removed a large portion of the Early Cretaceous sequence from the margins of the Basin (Rogers 1995). Of particular interest is the upper Pyap Member of the Monash Formation which can be correlated with the lowermost part of the Bulldog Shale in the Eromanga Basin (Rogers 1995). As previously mentioned the Eromanga basin has some of the highest temperature gradients recorded in Australia and areas with a similar thermal conductivity provide likely targets for geothermal exploration.

The uppermost sequence is the Paleocene to Quaternary age Murray Basin which covers 300,000 km^2 in southeastern SA, southwestern NSW and northwestern VIC. The succession has a thickness of up to 600 m with the thickest part occurring between Renmark and northwestern VIC. The Tertiary sediments are divided into three sequence sets: Late Paleocene to Early Oligocene non-marine and marginal marine sediments, Late Eocene to Middle Miocene transgressive marine sediments and Latest Miocene to Late Pliocene marine, coastal and non-marine sediments (Rogers *et al*. 1995).

Thermal conductivity tests of the Berri North 1, Monash 1 and Cooltong 1 (Figure 3) drill holes resulted in a thermal conductivity of 3.19 ± 0.14 W/mK for Devonian/Kanmantoo sediments, 2.66 ± 0.26 W/mK for the Urana Formation and an average of 2.1 ± 0.16 W/mK for the Monash Formation sediments (Bendall pers. com. 2009). These values are within the range of the average thermal conductivity (1.5-2.5 W/mK) required for a good geothermal resource.

2.2 Previous Geophysics in the Renmark Trough

Several geophysical methods have been used previously in the region including gravity, magnetics and seismic reflection. The latest (2007) gravity and magnetic grids (gridded at 100 m) for the Renmark area were supplied by Primary Industries and Resources South Australia's (PIRSA) SARIG website and input into Oasis Montaj. Figure 3 shows the gravity for the Renmark Trough, the black circles showing the site density and Figure 4 shows the TMI magnetic image. The gravity low of the basin is inferred to be caused by thicker sediments and the magnetic image shows a broad magnetic high beneath the basin. As the broad high is most likely due to a very deep and regional feature magnetics were not used in constraining the MT. Three gridded gravity transects were chosen across the Renmark Trough. Two of the transects coincide with RM01 and RM02 MT survey lines collected for this case study.

The 2D seismic reflection surveys were analysed using the Kingdom software package. PIRSA was contacted directly to retrieve the surveys for the Renmark Trough area with updated header location information in Seg-y format. The main seismic survey used was 65 MU 03, collected in 1965 but surveys carried out in the 1980's including 86 MU 01, 87 MU 01, 81 MU 01, 83 MU 01 and 85 MU 01 were also consulted during interpretation (Figure 4). The starting number of each survey indicates the year it was collected and all location information refers to GDA94, zone 54. Well logs for Overland Corner 1, Cooltong 1 and North Renmark 1 were used to produce time-depth tables and manufacture well ties. The seismic sections of two of the main seismic lines used in interpretation, 1965-R1 and OC85-22, are shown in Figure 5. The 1965 survey data were of poor quality with no reliable resolution at basement depth. However, there is a

very strong reflector, horizon A, in the middle of the Cretaceous sediments that was present in almost all seismic surveys in that area (well tie horizons were difficult to trace laterally due to poor data quality of surveys). The 1980's seismic surveys in the south of the trough clearly show a deep basement reflector, horizon B, seen especially well on line OC85-22. This is the only line which covers the cross section of the basin with enough data quality to image both horizons. However at the approximate point where MT station RM0110 crosses the seismic line, the basement reflector disappears in noise and the fault position is defined by the top reflector only. The Hamley fault appears to splay to the south west of the 1965-R5 line.

3. FIELD SURVEY, DATA ACQUISITION AND PROCESSING

3.1 Magnetotelluric and Geomagnetic Depth Sounding Theory

Magnetotellurics (MT) is a passive electromagnetic technique that uses the Earth's naturally varying magnetic and electric fields to explore resistivity structures within the subsurface rocks (Cagniard 1953; Vozoff 1972). The source of the variations is produced by the interaction of solar wind with the Earth's external magnetic field, which produces changes causing magnetic storms, diurnal fields, electric currents flowing through the ionosphere and electrical storms. Time-varying magnetic fields penetrate through the Earth, and induce an electrical response from the rocks at depth. The resulting variations in the magnetic and electric fields due to these secondary responses allow the electrical conductivity of the earth to be inferred.

Different magnetic sources will yield a different range of periods, each penetrating to varying depths within the Earth. The lower limit of depth resolution or penetration is known as the skin depth (δ). This is the depth (m) to which the field is attenuated to 1/*e* (~37%) of its maximum amplitude (Jones 1999). The skin depth is governed by the equation (1):

$$\delta = \sqrt{\left(\frac{\rho T}{\pi \mu 0}\right)} \qquad (1)$$

Where ρ is resistivity (Ωm), T is period (s) and μ_0 is the magnetic permeability of free space (4π x 10^{-7} N/A^2). Hence long period responses are sensitive to deeper structures. Generally, the period-bandwidth of MT measurements utilizes low frequency waves with periods in the range 0.001 to 10000 s, reaching depths of up to 500 km. This incorporates what is known as the dead band (1-10 s) that contains little natural sources of energy.

Magnetotelluric sounding, first introduced by Cagniard (1953), is a diffusive technique based on Maxwell's equations. The MT method simultaneously records time-series measurements of orthogonal horizontal components of the electric ($\mathbf{E}_x$, $\mathbf{E}_y$) and magnetic ($\mathbf{B}_x$, $\mathbf{B}_y$) variational fields (Simpson & Bahr 2005). The **B** and **E** orthogonal components are related in the frequency domain through the complex impedance tensor **Z**:

$$\begin{bmatrix} Ex \\ Ey \end{bmatrix} = \begin{bmatrix} Zxx & Zxy \\ Zyx & Zyy \end{bmatrix} \begin{bmatrix} Bx \\ By \end{bmatrix} \qquad (2)$$

Each element within the tensor is associated with an impedance phase angle (i.e. the lag between the electric and magnetic fields) defined by equation (3):

$$\theta = \arctan(Z_{ij}) \qquad (3)$$

The apparent resistivity ρ_a (a depth weighted average of all resistivities to approximately the skin depth), can be derived from the elements in the impedance tensor using equation (4):

$$\rho_a = \frac{2*10^{-7}}{T}\left|\frac{Ei}{Ej}\right| = \frac{2*10^{-7}}{T}|Z_{ij}|. \qquad \textit{Where } i = x, y \textit{ and } j = x, y$$

(4)

Geomagnetic depth sounding (GDS) is based on all three components of the magnetic field ($\mathbf{B}_x$, $\mathbf{B}_y$, $\mathbf{B}_z$). $\mathbf{B}_z$ is related to the horizontal magnetic fields through the tensor **T**:

$$[B_z] = [Tzx \quad Tzy] \begin{bmatrix} Bx \\ By \end{bmatrix} \tag{5}$$

As the tensor T is period dependant, induction arrows can be produced for different periods, indicating lateral changes in conductivity structure. Induction arrows (both real and imaginary) show the regional resistivity distribution but are only sensitive to lateral resistivity variations (Jones 1988). In the Parkinson convention (Parkinson 1962), real arrows point away from resistive areas and towards zones of higher conductivity.

For a 1D Earth (resistivity only changes with depth) the elements from equation (2) are such that $\mathbf{Z}_{xx} = \mathbf{Z}_{yy} = 0$ and $\mathbf{Z}_{xy} = -\mathbf{Z}_{yx}$. In the 2D Earth where resistivity changes with depth and one horizontal dimension, the tensor can be rotated by angle φ to align the observed electric and magnetic fields parallel (*x'*) and perpendicular (*y'*) with geomagnetic strike in the area. In this rotated *x'* and *y'* co-ordinate system the rotated elements $\mathbf{Z}_{x'x'} = \mathbf{Z}_{y'y'} = 0$ but generally the magnitude of $\mathbf{Z}_{x'y'} \neq \mathbf{Z}_{y'x'}$ (Simpson & Bahr 2005). In a 3D Earth the elements vary independently, and there is no relationship between them. As $\mathbf{B}_z = 0$ for a uniform or layered earth, the GDS tensor (5) only applies significantly to 2D and 3D structures.

For the 2D case, where the axis are aligned parallel and perpendicular to geomagnetic strike, electromagnetic fields decouple into two independent modes. The transverse electric (TE) mode has the tensor component $\mathbf{Z}_{x'y'}$ with the electric field along the strike of the structure (*x'*) and the magnetic field across the strike (*y'*). The transverse magnetic (TM) mode has the component $\mathbf{Z}_{y'x'}$ with the electric field across the strike (*y'*) and the magnetic field along the strike (*x'*) (Chakridi *et al*. 1992; Simpson & Bahr 2005).

3.2 Renmark Magnetotelluric and GDS Acquisition Survey and Processing

The survey consisted of 25 MT sites along two parallel survey lines (within the SAHFA) located on Calperum and Taylorville Stations, 5 km northwest of Renmark from the 19th May to the 27th May, 2009. One 38.5 km transect, denoted RM01, of broadband (100-0.01 Hz) data and one 35.3 km transect, denoted RM02, of long-period (10-10,000 s) data, around 10 km further to the north, were acquired. The transects are south-eastward trending. The survey was organised such that at least three stations were set up to record simultaneously to allow the use of Gamble *et al.*'s (1979) remote referencing technique where necessary. Tenement and site locations are shown in Figures 3 and 4 and Table 1.

The broadband line, RM01, had sites RM0108-RM0113 left out for a time longer period, as deeper imaging was required over the deepest part of the basement. The Broadband instruments have an operational (full) bandwidth and an effective (recorded) bandwidth, by leaving the instruments out longer the effective bandwidth is increased. The data were recorded at 500 Hz and were later down sampled to 1 Hz to extend the computed bandwidth response. The sites were recorded for 50 hours on average with the deepest parts of the basin recording around 70 hours of data. MT stations were spaced at 2-3 km intervals. This spacing was chosen as a compromise between covering the main basin structure and to ensure enough spatial resolution for mid- to upper-basin regions. Line RM01 was recorded where possible over the same track as seismic lines 1965-R1, in order to allow direct comparison and correlations between the data imaged by the two different geophysical techniques. Each station recorded two orthogonal components of the electric field in geomagnetic co-ordinates and the two orthogonal horizontal components of the magnetic field. Electric dipoles, place at right angles to each other (towards magnetic north and magnetic east), consisting of ceramic pots filled with saturated copper sulfate solution, were 50 m in length. When deployed, instrumentation and wiring were buried to prevent interference by animals and temperature distortions. The processed data from every second site are shown in Figure 6a.

The long-period line, RM02, was deployed to test the utility of long-period MT for geothermal application and to provide a parallel profile and investigate deep structure. Line RM02 used instruments developed by the University of Adelaide to recorded data at 10 Hz, which were then averaged into blocks of 1 s giving responses between 10-3000 s. Each site recorded just over 40-90 hours of data. MT stations were spaced at 4-5 km intervals. Each station recorded two orthogonal components of the electric field in geomagnetic co-ordinates and also three components of the magnetic field, as the vertical magnetic field was measured for RM02 sites to produce induction arrow data. The electric dipoles, placed at right angles to each other, were 20 m in length. The processed data of eight evenly distributed sites is shown in Figure 6b.

Processing for the Renmark Trough data was applied using Chave and Thomson's (1987, 2003, 2004) Bounded Influence Remote Reference Processing (BIRRP) code. Noisy data produced when crew were deploying and retrieving instrumentation was removed before processing. Broadband instruments (Line RM01) had their files catenated together and long-period instruments (Line RM02) had their fields catenated and re-sampled to 1 s. Variations of remote referencing, self-referencing and coherence thresholds were applied to remove random and coherent noise in the data and to boost signal in the dead band. Table 2 shows the different processing parameters applied to each site. Due to the large amount of data collected for each station (2.5-3 days worth) further processing was applied to broadband data. Using an averaging program the data for each station were re-sampled from 500 Hz to 1 Hz and processed using BIRRPs to deduce longer periods from the data. The final product was produced in edi format and in geographic co-ordinates.

3.3 Magnetotelluric Response

Two profiles of data were collected along profiles orientated perpendicular to the Hamley Fault, providing a cross section of the Renmark Trough and also allowing the simple mathematical rotation of the tensors to the major regional structure of the Hamley Fault. The MT response showed that at all sites the TE mode and TM modes were consistent in phase and the morphology of the apparent resistivity curves were the

same, though only consistent between sites on the same line. Figure 6 shows the comparison of the TE and TM mode MT responses (with 2D model inversion fits) from eight sites on line RM01 and eight on line RM02

The turning point in the apparent resistivity values from decreasing resistivity to increasing resistivity indicates the influence of a resistive basement structure. Between the sites on line RM01 the actual apparent resistivity values of the TE mode all have the same consistent trend with the maximum value in the 10^1-10^2 s period decreasing slightly in value systematically from north western to south eastern sites (Figure 6a). Site RM0105-RM0110 show a marked difference from the other sites with the turning point, most likely basement structure, occurring at periods of ~10^1 rather than the 10^0 of the deeper penetrating sites. This indicates a shallower basement along RM0105-RM0110 in comparison to sites northwest of them. The small variations in apparent resistivity could be due in a small way to static shift (a uniform shift in apparent resistivity as a result of near surface inhomogeneities that alter the electric field) or is possibly it is due to natural variations in sediments across the profile of the basin. Similar trends are seen in the TM apparent resistivity values of line RM01, though the TM mode has much more similar values between sites below 10^1 s period than the TE mode indicating a possibly more homogeneous medium in the TM mode orientation. The northern RM02 line follows a similar trend with the TE and TM mode apparent resistivity consistently decreasing from the northwest to southeast sites.

The TE and TM mode phases are often used as a diagnostic tool to infer the dimensionality of the structure below the sites (Mareshal *et al.* 1995; Simpson 2001). When the two phases overlap it implies that the earth is 1D, where as if the modes are split this implies a 2D, 3D or 1D anisotropic earth (Simpson & Bahr, 2005). For sites RM0111-RM0119 the phases overlap for periods up to 10^0 suggesting that the surface structure is 1D and then goes into a large split between 10^0 and 10^2 s. This suggests a 2D or anisotropic earth. For sites RM0105-RM0110 the phases do not split over the measured bandwidth indicating a more 1D earth to the southeast. For RM02, sites RM0220-RM0225 have a split in phases which appears to overlap once again at the

period of 10^3. The southeastern sites RM0226-RM0229 show approximately overlapping phases across the entire bandwidth, similar to the RM01 line trend.

All sites in RM01 display TE mode apparent resistivity values that cross from greater than the TM mode resistivities to less than the TM mode resistivities in the period range 10^0-10^1. The RM02 sites do not show that distinctive turning point indicating the basement structure due to the bandwidth of the instrument. This indicates that the resolution of the basement depths may be less for the long period data than the broadband data and that the broadband instruments may produce a more accurate and resolved image of shallow, prospective geothermal basins.

4. RESULTS AND DISSCUSSION

4.1 MT Modelling and Inversion

Results of the 2D smooth inversions of all the TE, TM and GDS data are given in Figure 7 for the RM01 and RM02 lines respectively. The WinGLink 2D inversion used the non-linear conjugate gradient method of Rodi and Mackie (2001), which simultaneously fits the data and minimises structure to yield the smoothest depth profile section that is structurally simple. The tau parameter, also known as the smoothness parameter, sets the balance between model smoothness and how accurately the data are fitted. These inversions contained error floors of 5 %, a tau parameter of 5 for RM01 and 3 for RM02, and these profiles had an RMS of 2.2 and 1.7 respectively. Horizontal smoothing of 1.2 was applied to both profiles. The model fits are shown on the processed data on Figure 6.

The RM01 and RM02 profiles are co-located with the gravity profiles shown in Figure 3. They were positioned perpendicular to the Hamley Fault. The main structures are labelled A-D on Figure 7. Structure A has a low resistivity (0.3-3 Ωm). It deepens from around 700 m to 1200 m to the southeast in RM01 and is equidistant from the higher resistivity basement along the profile of RM02. This grades into the slightly more resistive B structure which appears to define the position of the lower most conductive

sediments in the basin (3-10 Ωm). The thin area of around 11-12 Ωm (white blocks) defines the boundary between the less resistive sediments and the much more resistive (40-100 Ωm) basement (structure C). As such this boundary between structures B and C appears to change depth from the southwestern RM01 profile to the northeastern RM02 profile. However, the lack of resolution of the long-period data at that depth makes exact positioning of the basement boundary less certain than the boundary provided by broadband. Note that it is unknown if there are granites in the basement of the Renmark Trough and as such when referring to basement it is meant as crystalline basement and not as basement granite.

RM01 shows a deeper basin of 4 km at the point where the basin intersects with structure D interpreted to be the Hamley fault, a high angled structure separating sediments from basin, and then shallows to ~2.1 km for sites RM0105-RM0110. The boundary has a half-graben structure with a pronounced dip near the fault. To the west of the fault (RM0114-RM0119) the basement appears at around 700 m and deepens to 1000 m in the west. Even though the model has been smoothed the basement still appears to be eroded to the west of the fault.

RM02 (Figure 7b) appears to show a shallower basement at around 3-3.5 km in depth from RM0115-RM0229, delineating a graben structure. The apparent shallowing of basement to the north is quite possibly an artefact of the lack of resolution in RM02, as such the basement structure appears to be more graben than half graben by line RM02. The less resistive basin under RM0225-RM0228 is most likely an artefact of the inversion smoothing as is the deepening conductive structures on either end of the profile. The rise in basement depth between RM0228 and RM0229 could be an artefact of the inversion or possibly the very southern tip of the Chowilla fault however resolution is not good at this depth.

The specific locations of such features as the Hamley Fault (structure D) are hard to precisely define for several reasons: 1) The boundary is dependant on the site density. 2) The inversion smooths discontinuities in resistive values so as to blur the location of the boundary and 3) the MT/GDS methods are volume sounding techniques hence the

longer the period recorded the larger the volume sampled, hence a site away from the boundary may still contain signals associated with the boundary.

The resolution of the broadband RM01 profile produces a clearer image of the basin at 3-4 km depths than the long-period RM02 profile. This higher resolution and more homogenous image indicates that broadband is more suited to geothermal exploration though long-period MT can be used as a check on the continuation of basement structure. The long-period RM02, though low resolution, produced similar structures to RM01 and gave confidence to the notion that the inversions image a 2D structure.

4.2 Induction Arrow Response

The induction arrows, only produced on line RM02 provide little additional information. There is little change in the magnitude of the arrows along the profile indicating a relatively uniform crust and upper mantle throughout the length of the profile (Simpson & Bahr 2005). The arrows point to the southwest and all arrows are consistently small at all periods. This implies no major lateral variations in resistivity (Simpson & Bahr 2005).

4.3 Seismically Constrained Gravity Modelling

Horizons A and B were picked and gridded in Oasis Montaj before being input into the GM-SYS program. Average velocities of 2400 m/s, 4500 m/s and 6500 m/s from time-depth curves were used to convert the horizons to depth. Using the general lithologies from the well logs and considering the very low velocities recorded in the wells, lower limits on densities were determined and used to forward model the gravity curves along the RM01 (1965-R1 survey) line and also along the OC85-22 survey line which gave a more complete seismic cross section. The gravity models are shown in Figure 7. Though the gridded horizons do not fit the gridded gravity data exactly due to possible complications around the fault area, a half-graben structure with a deepening angle to 4 km fits the gravity data reasonably.

4.4 Integration and Interpretation of MT with Gravity and Seismics

There are several instances of combining geophysical methods in an effort to constrain and identify similarities between methods. For example it has become apparent that the onset of low resistivity in the crust often coincides with zones of relatively high seismic reflectivity (Gough 1986; Hyndman & Shearer 1989; Jones 1992). Methods such as the GDS measurements from RM02 only provide the approximate depth determination of the base of conductors (due to lower resolution) and as such other geophysical methods that give similar depths add confidence to such estimates. A useful check method is gravity, though the interpretation is non-unique in terms of modelling. The link between properties of seismic and gravity has been well exploited in the past. Similarly, there should be a strong link between gravity and MT as they are both sensitive to basin and basement structures.

Three forward model transects were constructed, as shown in Figure 3, in GM-SYS , using interpolated data from the PIRSA gravity grid along the transects. Densities were chosen from well log descriptions of sedimentary sequences and as indicated by the low seismic velocities. The sedimentary basin structure was modelled using well logs and seismic data as constraints. RM03 (Figure 9a), the north most profile and the one not analysed by MT, is easily modelled as a graben with the Chowilla fault forming another graben/half graben to the southeast. In this profile the graben is only around 2.4 km in depth. Similarly for RM02 (Figure 9b), when using the depths given by the MT model the gravity data were modelled very closely as a graben structure of 3.5 km in depth. Modelling RM01 (Figure 10a) with the MT model depths produces an ill-fitting gravity profile. Maintaining the geometry desired by MT requires sediments to be at unrealistically low densities for a good data fit. Hence this model may not be giving a complete picture.

When comparing the MT model with the seismic there is a very good correlation between the highly conductive structure A and the top reflector horizon A picked in the mid Cretaceous. They are both at similar depths and display the similar characteristic of deepening to the southeast. However, in the seismic it is clear that the basement (horizon B) is a low gradient dipping reflector that gradually deepens to the northwest.

The seismic horizon B and the MT basement are of a similar depth to the northwest of the Hamley Fault, yet the unconstrained MT model shows a clear deep bulging dip at the base of the fault before it rises quickly and plateaus out.

The MT model was rerun with a fixed basement resistivity structure, similar to that shown in the seismic, to test the MT model's reaction to this structure. This structure was applied to the initial unconstrained MT model (of RMS 2.2, horizontal smoothing of 1.2 and tau 5). The iterations were run for a variation of fixed parameter tau values. In this instance the tau value determines how fixed the model holds the resistivity structure that has been imputed, during the iterative model calculation process. Below a certain tau value the RMS reached a stable value and the final modified model is shown in Figure 11a and reached an RMS value of 2.2.

The RMS of the seismically constrained MT model is the same as the unconstrained model indicating that the MT model fit is unaffected by the seismically defined basement structure. The basement still reaches a maximum depth of 4 km and the conductive sediment fills in the more constrained basement, though structure B still maintains the shape of the initial MT model. Structure E fills in the space between structure B and the fixed basement. The new MT model depths added to the gravity model (Figure 10b) allow a closer fit of the gravity data along the length of the profile.

Comparing the gravity and MT of the constrained and unconstrained models several things can be concluded:

1. The deep dip near the fault of the unconstrained model fits the northwest half of the profile well, where as the seismically constrained model basement fits the southeast half of the profile better.
2. The pronounced dip in feature B is consistent in both constrained and unconstrained MT models. As a consequence of fixing the basement in the constrained model, structure E is produced. Magnetotellurics and seismics rely on different properties to produce their images, MT on resistivity (a diffusive technique) and seismics on acoustic impedance (which relies upon density). MT

resistivity is affected by porosity and permeability among other factors. Structure E appears to correspond to the Devonian sand layer illustrated in Figure 11b (a cross-section produced from drill holes and seismic). In this figure, there is a distinct dip (similar to structure B) of the above layer into the Devonian. A plausible explanation for structure E is that it forms a low permeability package in the area between the unconstrained and constrained MT model basements. Structure E would then be the area at which the porosity of the sand no longer interconnected, restricting percolation of fluid and hence producing higher resistivities, though the sediment is not part of the basement.

3. Long-period RM02 data fit the seismic grid well. Lower resolution could allow a similar shape to the seismic as the model is less sensitive to irregularities in porosity and permeability.

4.5 Thermal Modelling from 1D Resistivity Profile

The use of resistivity measurements for geothermal applications, other than exploration of subsurface geometry, has been minimally explored. Theoretically, as resistivity depends on several factors, such questions as is there fluid present and what useful additions can be made to temperature modelling, should be attainable from resistivity measurements.

Many drill holes in the continental crust has produced aqueous solutions in large amounts indicating aqueous solutions and fluids are wide spread in the upper/middle crust (Nesbitt 1993). As such the resistivity and position of fluids play a significant role in MT images particularly as sedimentary basins often contain fluids. The presence of fluids near the basement is important for the creation of more economic hot wet rock geothermal systems. An important application of MT is to determine if the resistivity profile data can provide fluid information.

Porosity decreases exponentially (Bahr *et al.* 2001) during the burial and compaction of marine sediments which in turn decreases conductivity. However at the same time there is an increase in fluid conductivity at depth due to an increase in temperature (Heinson

pers. com. 2009). The basement underlying a geothermal basin can be assumed to have essentially zero porosity. At depths of 3-4 km it is unknown at this time whether the resolution of MT is such that the difference could be told between a section of sediment decreasing in conductivity due to reduction of porosity and fluid but an increase in temperature, or due to a fractured basement containing fluid. The change in response may not be large enough to detect at these depths, however, this is a topic of ongoing research (Thiel pers. com. 2009).

In an attempt to model temperature gradient within the Renmark Trough using resistivity measurements, three 1D resistivity models of four, five and six layers were constructed in WinGLink for three sites over the deepest section of the Trough, RM0113-RM0111 respectively (Figure 12a). Common to all three profiles was a minimum resistivity at a depth of 300-500 m. This turning point is unusual but significant, as the position of the turning point stays fixed through various model iterations even though the resistivity of the layers varied for each iteration. With no other constraints in the area from well logs to identify a possible explanation for the turning point, it may be feasible to model temperature gradient using this feature.

Porosity, salinity and temperature are all unknowns in this area as relevant logs were not recorded in any wells near the trough and the amount of variation between wells on either side of the trough is unknown. To calculate the bulk resistivity and hence give an estimate of the temperature gradient range, the salinity of the area (hence water resistivity) and the porosity must be assumed in this area. It has been noted by Bahr *et al.* (2001), using a database of worldwide marine core samples, that porosity generally decreases as an exponential function with depth. Only cores, which contained a majority of sand, shale or silt, were included in the study and each core was placed in one of the three respective groups accordingly. The equations for sand, shale and silt for the porosity of these marine cores provide an upper limit for general porosity with depth as these cores tend to have the most unconsolidated sediments. This only provides an upper limit and the rate at which the porosity decreases in the trough sediments is unknown. The equations below are those used by Bahr *et al.* (2001) for sand, shale and silt respectively:

$$por(depth) = 0.617 \times \exp(-5.55e^{-4} \times depth) \quad (6)$$

$$por(depth) = 0.630 \times \exp(-5.71e^{-4} \times depth) \quad (7)$$

$$por(depth) = 0.803 \times \exp(-7.95e^{-4} \times depth) \quad (8)$$

The first constant is the surface porosity and the second constant dictates the rate of compaction. For simplification it has been assumed that salinity is constant. The surface water resistivity ($\rho_{surface}$ =2 Ωm for this model) has been calculated by extrapolating the y-intercept of the TE/TM mode data curves, in Figure 6, as the bulk resistivity and rearranging the simplified Archie's law below to retrieve ρ_{water}:

$$\rho_{bulk} = \rho_{water}\, \Phi^{-2} \quad (9)$$

Where ρ is resistivity and Φ is the porosity. Equations for the resistivity of depth (10) and Archie's law for bulk resistivity (11) were then used to produce the depth vs. temperature gradient and resistivity plots in Figure 12b.

$$\rho_{water} = 1/(1/\rho_{surface} + T/10) \quad (10)$$

$$\rho_{bulk} = \rho_{water} \times a \times por(depth)^{-m} \quad (11)$$

Where T is temperature and a and m are the constants for Archie's law. Complete saturation is assumed and constant values used are taken from a table by Keller (1987) for different lithologies.

Figure 12b shows depth vs. temperature gradient plots with bulk resistivity isotherms for sand, shale and silt respectively, for three different sets of Archie's constants. The first set is for a porosity range from 25-45%, generally of Tertiary age, the second set for a porosity of 18-35%, generally of Mesozoic age and the third set for a porosity of 5-25% usually of Paleozoic age (Keller 1987). Note the turning point of the resistivity isotherms are reasonably invariant. By matching the depth of the turning point for the isotherms to the depth of the turning point in the 1D resistivity profiles, it may be possible to constrain a temperature gradient range. A decrease in porosity from the first

to the third set allows the turning point to become shallower. The closest turning point near 500 m is the silt plot in the third set. This suggests that the porosity of the trough is much less than the upper limit marine sediment equations.

The lithological log of Cooltong 1 (the deepest and closest well bore; Figure 12a) indicates that the top 980 m of the trough is Tertiary sediments. As the turning point is within this package the Archie's constants for sediments of Tertiary age were used to further constrain the approximation. The stratigraphic log indicates that the main sediments in this package are sandstones and limestone in the lower section. The lithological log for North Renmark 1 (Figure 12a) however, shows a majority of silt rather than sandstone. Figure 12c shows the results of the manipulation of the compaction rate constant in the porosity equations for both sand and silt. By changing the porosity equations for sand and silt so that the sediments essentially compact faster, the turning point of the resistivity isotherms in Figure 12c becomes shallower at larger constants. At constants of ~ -14.9 the turning point of the isotherms for both sand and silt are at a similar height to the minimum resistivity in the 1D profiles in Figure 12a. The average minimum resistivity in the profiles ranges from 1.1 - 0.7 Ωm. From the plots in Figure 12c it could be inferred that the temperature gradient range for a mainly sand based trough is 75-110 ºC/km and 50-75 ºC/km for a mainly silt based trough. The large range is due to the lack of constraints we can place on the area.

This process is a rough estimation of temperature gradient that could be attempted with caution when there are no other available constraints on the area. Here it is assumed porosity decreases exponentially with depth and hence that the sedimentary package is composed of one type of sediment. As shown in Cooltong 1 lithological log, this is not the case so the exponential decrease in porosity is not necessarily valid. We are also assuming complete saturation below the water table. One final aspect to consider is the possibility that the minimum resistivity turning point could be due to an aquifer at the turning point overlain by a less porous sediment or could be just a low resistivity clay layer. The well logs give no clear indication on these possibilities.

5. DISCUSSION AND CONCLUSION

The thick regolith cover, Tertiary Aeolian deposits, and lack of knowledge of tectonic and basement structure are impediments to exploration of the Renmark region. However the application of MT has added to the understanding of basement structure. Line RM01 shows an apparently eroded basement west of the Hamley Fault (structure D), shallowing from a depth of 1000 m to 700 m between RM0119-RM0114. East of the fault a half-graben structure is delineated, with a maximum depth of 4 km at the point where the basin intersects with the fault. Structure B of the unconstrained MT model then shallows to ~2.1 km for sites RM0105-RM0110, however, the seismically constrained MT model indicates the basement gradually shallows to a depth of 1.5 km by site RM0105. To the northeast, RM02 appears to image a shallower basement at around 3-3.5 km in depth from RM0115-RM0229, delineating a graben structure, though the shallowing of the basement may be due to the resolution of the long-period image.

Though any set of geophysical techniques can be compared, it must be considered how consistent the gravity, seismic and MT data are to each other. In the case of these three geophysical techniques the same contributing parameters do not apply to each method. Gravity is a non-unique method, dependant upon densities, which has a strong link to seismics (dependant on acoustic impedance, hence seismic velocities and density) which provides the most unique solution of the three methods. In this data set gravity sampling on RM01 is incomplete with several suspect data points near stations RM0112-RM0113. The seismic datasets are old and of poor quality and velocity estimates are speculative due to the age and position of local well bores. MT is a diffusive technique, dependant upon resistivity (subsequently porosity, salinity, temperature and fluids) and in comparison seismic depends on velocities which need to be properly recorded to provide accurate depth conversion.

Comparing seismic and MT is not a strictly accurate process as each method relies on different parameters. The MT method though non-unique (as shown by consistent RMS between constrained and unconstrained models) when constrained is able to identify

structure E, which appears to be a fairly resistive sediment indicating a low permeability, non-connected pore area. This is an additional piece of information which was not detectable using seismic. The reflective and wave interfering methods of the seismics causes the basement reflector horizon B, in such lines as OC85-22 (Figure 5b) to die out ~5 km from the fault. These interference properties of seismic do not allow the method to image the area near a high angle fault. Though the area around the fault is most likely complex, the MT resistivity parameters can provide a cohesive image of the area where seismic is liable to problems. This provides a confident estimate of 4 km maximum depth in a possibly seismically complex area. In terms of time and economic constraints, MT provides images of a similar depth and shape to that of seismic reflectors, and provides additional information particularly in possibly complex regions.

The temperature gradient calculated from 1D resistivity is a very rough estimate and for this area it is highly speculative. This method is assuming a linear temperature gradient. The compaction, burial, uplift and unconformities in the sediments of the trough would greatly impact the porosity equation for the area making the marine core sediment equations a poor estimate of the area's porosity. The Archie's Law constants vary greatly between different areas, the manipulation of the compaction constant is at most a test of the model parameters and the salinity may vary with depth. Also the temperature gradient range varies depending upon which sediment is more predominant, 75-110 ºC/km for sand (majority lithology in Cooltong 1) and 50-75 ºC/km for silt (majority lithology in North Renmark 1).

By using the turning point as a reference it has been possible to infer a potential temperature gradient. In principle if this model could be constrained in one place - for example, the appropriate well logs for salinity and porosity down a well bore close to or ideally in the trough - it would greatly help in constraining the rest of the tenement. It may be possible to use an Occam inversion from WinGLink to directly calculate a temperature gradient curve (non-linear) using well bore information (eg. Constable *et al.* 2009).

The geothermal exploration of the Renmark Tenement was ultimately aided by the use of MT to investigate the subsurface. Magnetotellurics allowed identification of basin geometry, imaged basin depth in a complex area that seismics failed to clearly define, identified a possible low permeability area and the survey cost was significantly lower than that of a seismic survey. Further more with additional information from relogging existent well bores and drilling new wells, the temperature calculations from 1D resistivity models can be better constrained and provide a guide to better temperature modelling in the future.

6. ACKNOWLEDGEMENTS

I would like to thank my major support my supervisor Dr Graham Heinson for his guidance, encouragement and scientific input. Thank you also to my associate supervisors Martin Hand (official) and Graham Baines (unofficial) for their contribution to the many different geophysical paths I took in the project. This also extends to the rest of the brilliant University of Adelaide MT personal especially Stephan Thiel, Kate Selway and Rachel Maier. I would like to thank Petratherm for the use of their tenement, their funding of the field work and the help and input of Louise McAllister and Peter Reid. Thanks also to Goren Boren and Jared Peacock for being my fieldies and technical support when I collected data in Renmark. Thanks also to the manager of Calperum and Talorville stations, Dr Grant Whiteman, for access to the area. A very heart felt thank you to my wonderful family and partner for their support through the crazy times. Finally thank you to the University of Adelaide, School of Earth and Environmental Sciences for the opportunity to complete honours.

7. REFERENCES

ALLEY N.F. & GRAVESTOCK D.I. 1995. The geology of South Australia. Vol. 2, The Phanerozoic: Middle Palaeozoic (Devonian): Darling Basin. *South Australia Geological Survey. Bulletin* **54**, pp 44.

ALLEY N.F. 1995. The geology of South Australia. Vol. 2, The Phanerozoic: Late Palaeozoic: Nadda Basin. *South Australia Geological Survey. Bulletin* **54**, pp 70.

BAHR D.B., HUTTON E.W.H., SYVITSKI J.P.M. & PRATSON L.F. 2001. Exponential approximations to compacted sediment porosity profiles. *Computers & Geosciences* **27**, 691-700.

BLOCK L.V., CHENG C.H., FEHLER M.C. & PHILLIPS W.S. 1994. Seismic imaging using microearthquakes induced by hydraulic fracturing. *Geophysics* **59(1)**, 102-112.

CAGNIARD L. 1953. Basic theory of the magnetotelluric method of geophysical prospecting. *Geophysics* **18**, 605-645.

CHAKRIDI R., CHOUTEAN M. & MARESCHAL M. 1992. A simple technique for analysing and partly removing galvanic distortion from the magnetotelluric impedance tensor; application to Abitibi and Kapuskasing data (Canada). *Geophysics Journal International* **108** (3), 917-929.

CHAVE A.D., THOMSON D.J. & ANDER M.E. 1987. On the robust estimation of power spectra, coherences, and transfer functions. *Journal of Geophysical Research* **92**, 633-648.

CHAVE A.D. & THOMSON D.J. 2003. A bounded influence regression estimator based on the statistics of the hat matrix, *Journal of the Royal Statistical Society: Series C, (Applied Statistics)* **52***,* 307-322.

CHAVE A.D. & THOMSON D.J. 2004. Bounded influence estimation of magnetotelluric response functions. *Geophysical Journal International* **157**, 988-1006.

CONSTABLE S., KEY K. & LEWIS L. 2009. Mapping offshore sedimentary structure using electromagnetic methods and terrain effects in marine magnetotelluric data. *Geophysical Journal International* **176**, 431-442.

CULL J.P. 1982. An appraisal of Australian heat-flow data. *BMR Journal of Australian Geology and Geophysics* **v.7**, 11–21.

DEBAYLE E. & KENNETT B.L.N. 2003. Surface-wave studies of the Australian region. In: Hillis, R.R. and Müller, R.D. (Eds), Evolution and Dynamics of the Australian Plate. *Geological Society of Australia Special Publication* **22** & *Geological Society of America Special Paper* **372**, 25–40.

DUCHANE D.V. 1994. Status of the United States hot dry rock geothermal technology development program. *Geothermal Tech 1994* **19** (1 and 2), 12-30.

EVANS K.F., CORNET F.H., HASHIDA T., HAYASHI K., ITO T., MATSUKI K. & WALLROTH T. 1999. Stress and rock mechanics issues of relevance to HDR/HWR engineered geothermal systems: review of developments during the past 15 years. *Geothermics* **v. 28**, 455–474.

FEHLER M.C. 1989. Stress control of seismicity patterns observed during hydraulic fracturing experiments at the Fenton Hill hot dry rock geothermal energy site, New Mexico (abs). *International Journal of Rock Mechanics and Mining Science and Geomechanics Abstracts* **v. 26**, 211–219.

FISHWICK S., KENNETT B.L.N & READING A.M 2005. Contrasts in lithospheric structure within the Australian craton – insights from surface wave tomography. *Earth and Planetary science Letters* **231**, 162-176.

GAMBLE T., GOUBAU W. & CLARKE J. 1979. Magnetotellurics with a remote magnetic reference. *Geophysics* **44**, 53-68.

GOUGH D.I. 1986. Seismic reflectors, conductivity, water and stress in the continental crust. *Nature* **323**, 143-144

HEINSON G. & WHITE A. 2005. Electrical resistivity of the Northern Australian lithosphere: Crustal anisotropy or mantle heterogeneity? *Earth and Planetary Science Letters* **232**, 157-170.

HILLIS R., HAND M., MILDREN S., MORTON J., REID P. & REYNOLDS S. 2004. Hot Dry Rock Geothermal Exploration in Australia. *PESA Eastern Australaisian Basins Symposium II*, 413- 421.

HOUSEMAN G.A., CULL J.P., MUIR P.M. & PATERSON H.L. 1989. Geothermal signatures and uranium ore deposits on the Stuart Shelf of South Australia. *Geophysics* **v. 54**, 158–170.

HYNDMAN R.D. & SHEARER P.M. 1989. Water in the lower continental crust: Modelling magnetotelluric and seismic reflection results. *Geophysical Journal International* **98**, 343-365.

JONES A.G. 1988. Static shift of magnetotelluric data and its removal in sedimentary basin environment. *Geophysics* **53**, 967-978.

JONES A.G. 1992. Electrical conductivity of the continental lower crust. In *The Continental Lower Crust*, pp. 81-143, Elsevier, NY.

JONES A.G., KATSUBE T.J. & SCHWANN P. 1997. The longest conductivity anomaly in the world explained: Sulphides in fold hinges causing very high electrical anisotropy. *Journal of Geomagnatisim Geoelectricity* **49**, 1619-1629.

JONES A.G. 1999. Imaging the continental upper mantle using electromagnetic methods. *Lithos* **48**, 57-80.

KELLER G.V. & NABIGHIAN M.N. (Ed) 1987. Rock and mineral properties. In *Electromagnetic methods in applied geophysics - theory* **vol.1**. Society of Exploration Geophysicists, p.13-51.

KUSI R., WHITE A., HEINSON G., MILLIAN P. 1998. Electromagnetic induction studies in the Eyre Peninsula, south Australia. *Geophysical Journal International* **132**, 687-700.

MARESCHAL M., KELLETT R.L., KURTZ R.D., LUDDEN J.N., JI S. & BAILEY R.C. 1995. Archean cratonic roots, mantle shear zones and deep electrical anisotropy. *Nature* **375**, 134-137.

MCLENNAN S.M. & TAYLOR S.R. 1996. Heat flow and the chemical composition of continental crust. *Journal of Geology* **v. 104**, 369–377.

MORGAN P. 1984. The thermal structure and thermal evolution of the continental lithosphere. In: Pollack Henry, N. and Murthy, V. R. (Eds), Structure and evolution of the continental lithosphere. *Physics and Chemistry of the Earth* **v. 15**, 107–193.

NESBITT B.E. 1993. Electrical Resistivities of Crustal fluids. *Journal of Geophysical Research* **vol. 98**, no. B3, 4301-4310.

NEUMANN N., SANDIFORD M. & FODEN J. 2000. Regional geochemistry and continental heat flow; implications for the origin of the South Australian heat flow anomaly. *Earth and Planetary Science Letters* **v. 183**, 107-120.

NYBLADE A.A. & POLLACK H.N. 1993. A global analysis of heat flow from Precambrian terrains: implications for the thermal structure of Archean and Proterozoic lithosphere. *Journal of Geophysical Research* **v. 98**, 12,207–12,218.

O'BRIEN P.E. 1986. Stratigraphy and sedimentology of Late Palaeozoic glaciomarine sediments beneath the Murray Basin, and their palaeo-geographic and palaeoclimatic significance. *BMR Journal of Australian Geology and Geophysics* **10**, 53-63.

PARKINSON W.D. 1962. The influence of continents and oceans on geomagnetic variations. *Geophysics Journal of the Royal Astronomical society* **6**, 441-449.

REID P. & HAND M., 2005. Exploring for Radiogenic Heat. *Abstracts #78. 4th Sprigg Symposium. Uranium: Exploration, Deposits, Mines and Minewaste Disposal geology.* Geological society of Australia, SA Division.

ROGERS P.A. 1995. The geology of South Australia. Vol. 2, The Phanerozoic: Mesozoic: Jurrasic-Cretaceous Epicratonic Basins: Berri Basin. *South Australia Geological Survey. Bulletin* **54**, pp 127-129.

ROGERS P.A., LINDSAY J.M., ALLEY N.F., BARNETT S.R., LABLACK K.L. & KWITKO G. 1995. The geology of South Australia. Vol. 2, The Phanerozoic: Tertiary: Southern Marine Basins: Murray Basin. *South Australia Geological Survey. Bulletin* **54**, pp 157-163.

RODI W. & MACKIE R.L. 2001. Nonlinear conjugate gradients algorithm for 2-D magnetotelluric inversion. *Geophysics* **66**, 174-187.

SATO H. & MACKIE R.L. 1984. Low-Frequency Electrical-Impedance of Partially Molten Gabbro – The Effect of Melt Geometry on Electrical-Properties. *Tectonophysics* **107**, 105-134.

SHANKLAND T.J. & ANDER M.E. 1983. Electrical-Conductivity, Temperatures, and Fluids in the Lower Crust, *Geophysical Research Letters* **88**, 9475-9484.

SHAPIRO S.A., HUENGES E. & BORM G. 1997. Estimating the crust permeability from fluid-injection-induced seismic emission at the KTB site. *Geophysical Journal International* **v. 131**, F15–F18.

SIMPSON F. & BAHR K. 2005. *Practical Magnetotellurics*. Cambridge University Press, Cambridge.

SIMPSON F. 2001. Resistance to mantle flow inferred from the electromagnetic strike of the Australian upper mantle. *Nature* **412**, 632-635.

SOMERVILLE M., WYBORN D., CHOPRA P., RAHMAN S., ESTRELLA D. & VAN DER MEULEN T. 1994. Hot Dry Rocks Feasibility Study. *Energy Research and Development Corporation (ERDC) Report* **243**, 133 p.

TELFORD W.M., GELDART L.P. & SHERIFF R.E. 1990. *Applied Geophysics*. Cambridge University Press, Cambridge.

THORTON R.C.N. 1974. Hydrocarbon potential of western Murray Basin and infrabasins. *South Australia. Geological survey. Quarterly Geological Notes* **44**, 5-11.

VOZOFF K. 1972. The magnetotelluric method in the exploration of sedimentary basins. *Geophysics* **37**, 98-141.

WANNAMAKER P.E., HOHMANN G.W. & WARD S.H. 1984. Magnetotelluric responses of three-dimensional bodies in layered earths, *Geophysics* **49**, 1 517-511 533.

ZIELHUIS A. & VAN DER HILST R.D. 1996. Upper-mantle shear velocity beneath eastern Australia from inversion of waveforms from SKIPPY portable arrays. *Geophysical Journal International* **v. 127**, 1–16.

8. FIGURE CAPTIONS

Figure 1: The South Australian Heat Flow Anomaly, (shaded area, amended from Cull 1982; Neumann *et al.* 2000). Numbers are heat flow in milliW/m^2. Darker shading within SAHFA represents the extent of Neoproterozoic metasediments. Dashed lines represent inferred boundaries of Gawler and Curnamona Cratons. The black box shows the case study area.

Figure 2: Shows the relationship between depth of burial and temperature for a range of heat flows, and assuming a constant thermal conductivity (2 W/mK) of the cover sequence.

Figure 3: The gravity image for the Renmark Trough. The gravity and MT profiles are indicated at their ends by arrows. The black dots indicate the points where gravity data was collected. Petratherm tenement boundaries are in purple and station locations are in yellow.

Figure 4: The TMI magnetic image (broad flight lines) for the Renmark Trough. The yellow lines are the seismic lines for the area. Petratherm tenement boundaries are in purple and station locations are in red.

Figure 5: Seismic images for lines 1965-R1 and OC85-22. Picked horizons A and B are indicated by black and purple arrows respectively.

Figure 6: TE and TM mode data collected for each site and the model fits of the two MT profiles. a) Every second site for line RM01. Note the green line indicating the 45-degree phase value and the blue line denoting the apparent resistivity at the turning point. b) Eight selected sites for line RM02.

Figure 7: Figures labelled with main structures A-D. a) Unconstrained MT model for RM01 RMS = 2.2, tau=5, horizontal smoothing = 1.2. b) Unconstrained MT model for RM02 RMS=1.7, tau=3, horizontal smoothing = 1.2.

Figure 8: a) Gravity modelling of seismic line 1965-R1. b) Gravity modelling of OC85-22. Note in b) that all gridded gravity points are present and in part a) that gravity points due only to gravity grid interpolation have been removed to differentiate the real points that need to be modelled from the interpolated gravity points.

Figure 9: a) Gravity modelling of profile RM03. b) Gravity modelling of RM02 using basement depths given by the unconstrained MT model.

Figure 10: a) Gravity modelling of profile RM01 using basement depths given by the unconstrained MT model. b) Gravity modelling of profile RM01 using basement depths given by the seismically constrained MT model. Note in a) that all gridded gravity points are present and in part b) that gravity points due only to gravity grid interpolation have been removed to differentiate the real points that need to be modelled from the interpolated gravity points.

Figure 11: a) MT model of seismically altered profile RM01 RMS=2.2, tau=5, horizontal smoothing = 1.2. Structures A-E annotated in text. b) Cross-section of Renmark Trough from PIRSA's Bulletin 54 (Rogers 1995). The cross-section is derived from well bores and seismic images.

Figure 12: a) 4,5 and 6 layered 1D model fits of TE/TM data of RM0113-RM0111. The turning point occurs at depths of 300-500 m for resistivities of 1.05 – 0.7 Ωm. Also supplied are the lithological logs of drill holes Cooltong 1 (sand majority) and North Renmark 1 (siltstone majority). b) The depth vs. temperature gradient and resistivity plots for sand, shale and silt for three different Archie's constants. The porosity equations are those from Bahr *et al.* (2001). The first set are for generally Tertiary sediments, the second set for Mesozoic sediments and the third for Paleozoic sediments. c) Various compaction constants for sandstone and siltstone using Archie's Law constants for Tertiary sediments.

9. TABLES

Table 1

Station	Easting	Northing	Elevation (m)	Measured fields	Instrument used
RM0105	465257	6231637	44.4m	$\mathbf{E}_x,\mathbf{E}_y,\mathbf{B}_x,\mathbf{B}_y$	BB
RM0106	463322	6233207	60.4m	$\mathbf{E}_x,\mathbf{E}_y,\mathbf{B}_x,\mathbf{B}_y$	BB
RM0107	461851	6237237	59.4m	$\mathbf{E}_x,\mathbf{E}_y,\mathbf{B}_x,\mathbf{B}_y$	BB
RM0108	458974	6237167	44.9m	$\mathbf{E}_x,\mathbf{E}_y,\mathbf{B}_x,\mathbf{B}_y$	BB
RM0109	457094	6237157	37.8m	$\mathbf{E}_x,\mathbf{E}_y,\mathbf{B}_x,\mathbf{B}_y$	BB
RM0110	455255	6237910	61.9m	$\mathbf{E}_x,\mathbf{E}_y,\mathbf{B}_x,\mathbf{B}_y$	BB
RM0111	453175	6239397	42.1m	$\mathbf{E}_x,\mathbf{E}_y,\mathbf{B}_x,\mathbf{B}_y$	BB
RM0112	451246	6240780	45.5m	$\mathbf{E}_x,\mathbf{E}_y,\mathbf{B}_x,\mathbf{B}_y$	BB
RM0113	449413	6242087	63.3m	$\mathbf{E}_x,\mathbf{E}_y,\mathbf{B}_x,\mathbf{B}_y$	BB
RM0114	446837	6243917	83.4m	$\mathbf{E}_x,\mathbf{E}_y,\mathbf{B}_x,\mathbf{B}_y$	BB
RM0115	444847	6245337	74.3m	$\mathbf{E}_x,\mathbf{E}_y,\mathbf{B}_x,\mathbf{B}_y$	BB
RM0116	443368	6246381	59.2m	$\mathbf{E}_x,\mathbf{E}_y,\mathbf{B}_x,\mathbf{B}_y$	BB
RM0117	441557	6247970	63.2m	$\mathbf{E}_x,\mathbf{E}_y,\mathbf{B}_x,\mathbf{B}_y$	BB
RM0118	439439	6249091	66.5m	$\mathbf{E}_x,\mathbf{E}_y,\mathbf{B}_x,\mathbf{B}_y$	BB
RM0119	436905	6250023	58.3m	$\mathbf{E}_x,\mathbf{E}_y,\mathbf{B}_x,\mathbf{B}_y$	BB
RM0220	445908	6258728	63m	$\mathbf{E}_x,\mathbf{E}_y,\mathbf{B}_x,\mathbf{B}_y,\mathbf{B}_z$	LP
RM0221	450677	6254174	63.5m	$\mathbf{E}_x,\mathbf{E}_y,\mathbf{B}_x,\mathbf{B}_y,\mathbf{B}_z$	LP
RM0223	455504	6252315	47.5m	$\mathbf{E}_x,\mathbf{E}_y,\mathbf{B}_x,\mathbf{B}_y,\mathbf{B}_z$	LP
RM0224	458156	6252042	42.5m	$\mathbf{E}_x,\mathbf{E}_y,\mathbf{B}_x,\mathbf{B}_y,\mathbf{B}_z$	LP
RM0225	460969	6251708	51.5m	$\mathbf{E}_x,\mathbf{E}_y,\mathbf{B}_x,\mathbf{B}_y,\mathbf{B}_z$	LP
RM0226	465379	6249380	43.6m	$\mathbf{E}_x,\mathbf{E}_y,\mathbf{B}_x,\mathbf{B}_y,\mathbf{B}_z$	LP
RM0226b	464483	6246910	37.1m	$\mathbf{E}_x,\mathbf{E}_y,\mathbf{B}_x,\mathbf{B}_y,\mathbf{B}_z$	LP
RM0227	468800	6243807	57.1m	$\mathbf{E}_x,\mathbf{E}_y,\mathbf{B}_x,\mathbf{B}_y,\mathbf{B}_z$	LP
RM0228	471977	6241441	50.4m	$\mathbf{E}_x,\mathbf{E}_y,\mathbf{B}_x,\mathbf{B}_y,\mathbf{B}_z$	LP
RM0229	475478	6240719	31m	$\mathbf{E}_x,\mathbf{E}_y,\mathbf{B}_x,\mathbf{B}_y,\mathbf{B}_z$	LP

Table 1: Stations are of two types: BB-Broadband which use 2 magnetic coils and electrodes and LP- Long Period which use a magnetometer and 2 electrodes. All locations are in GDA94, zone 54, declination 8.724º.

Table 2

Station	Remote or Self Referenced?	Remote reference	Coherence threshold?
RM0105	RR	RM0106	
RM0106	RR	RM0105	
RM0107	RR	RM0105	
RM0108	SR		0.4
RM0109	RR	RM0110	
RM0110	RR	RM0109	0.2
RM0111	SR		
RM0112	RR	RM0113	0.3
RM0113	SR		0.4
RM0114	RR	RM0115	
RM0115	RR	RM0114	0.3
RM0116	RR	RM0115	
RM0117	SR		0.4
RM0118	SR		0.4
RM0119	RR	RM0118	
RM0220	RR	RM0223	0.3
RM0221	RR	RM0229	
RM0223	RR	RM0224	0.4
RM0224	RR	RM0225	
RM0225	RR	RM0224	
RM0226			
RM0226b	RR	RM0227	
RM0227	SR		
RM0228	RR	RM0227	
RM0229	RR	RM0221	

Table 2: Lists the processing applied to each site. Note that site RM0226 had bad **E** field data and hence is only used for induction arrows.

10. FIGURES

Figure 1

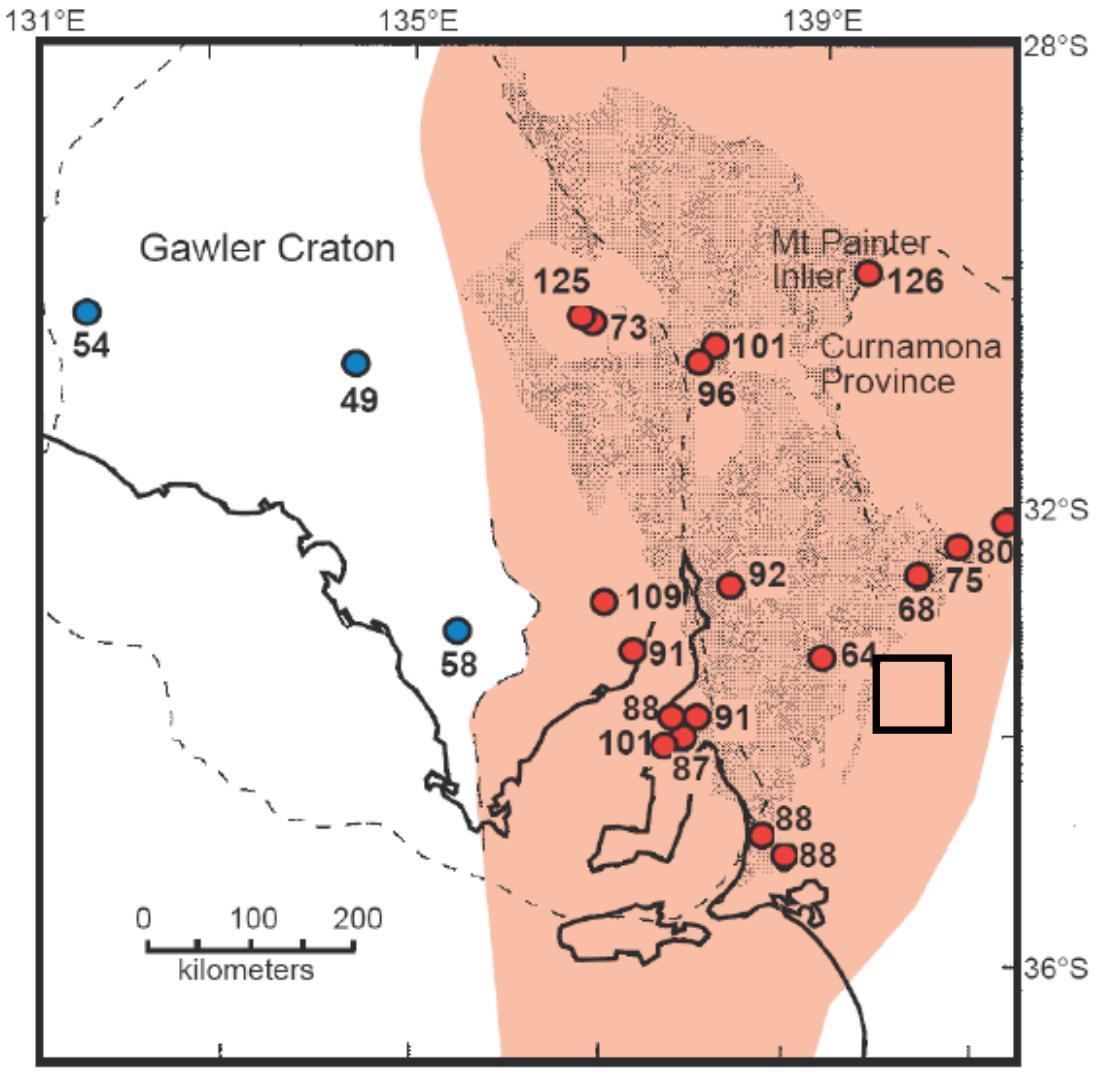

Figure 2

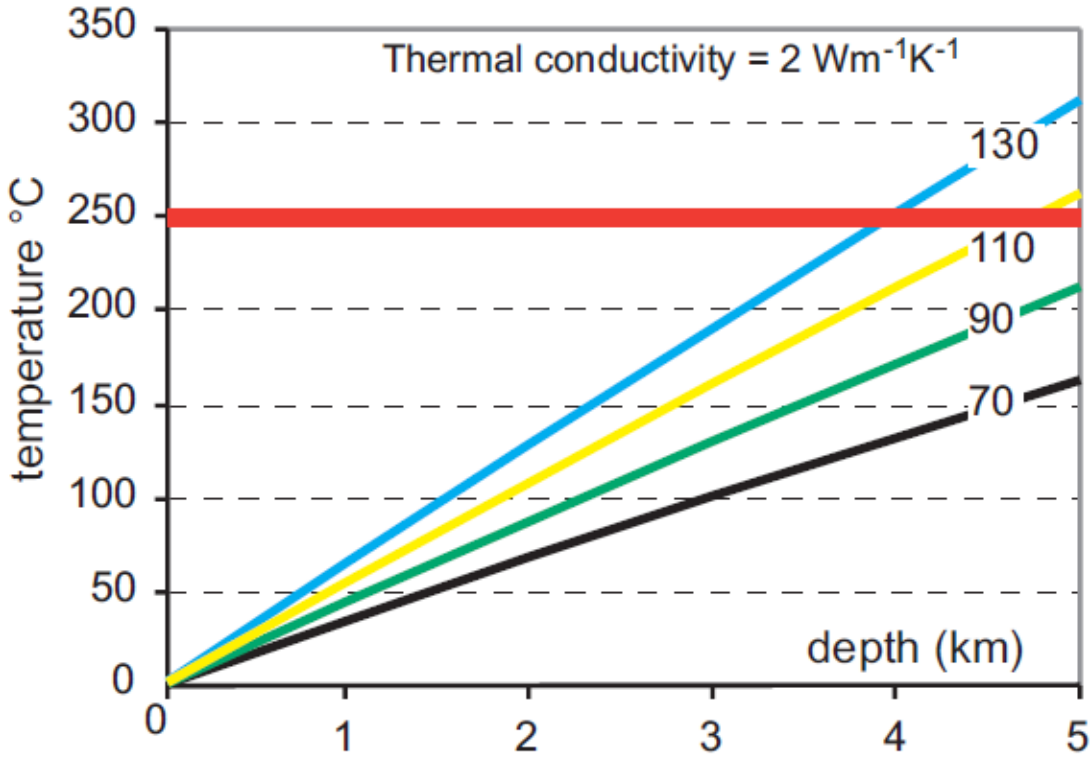
Thermal conductivity = 2 Wm-1K-1
130
110
90
70
temperature °C
depth (km)
350
300
250
200
150
100
50
0
0
1
2
3
4
5

Figure 3

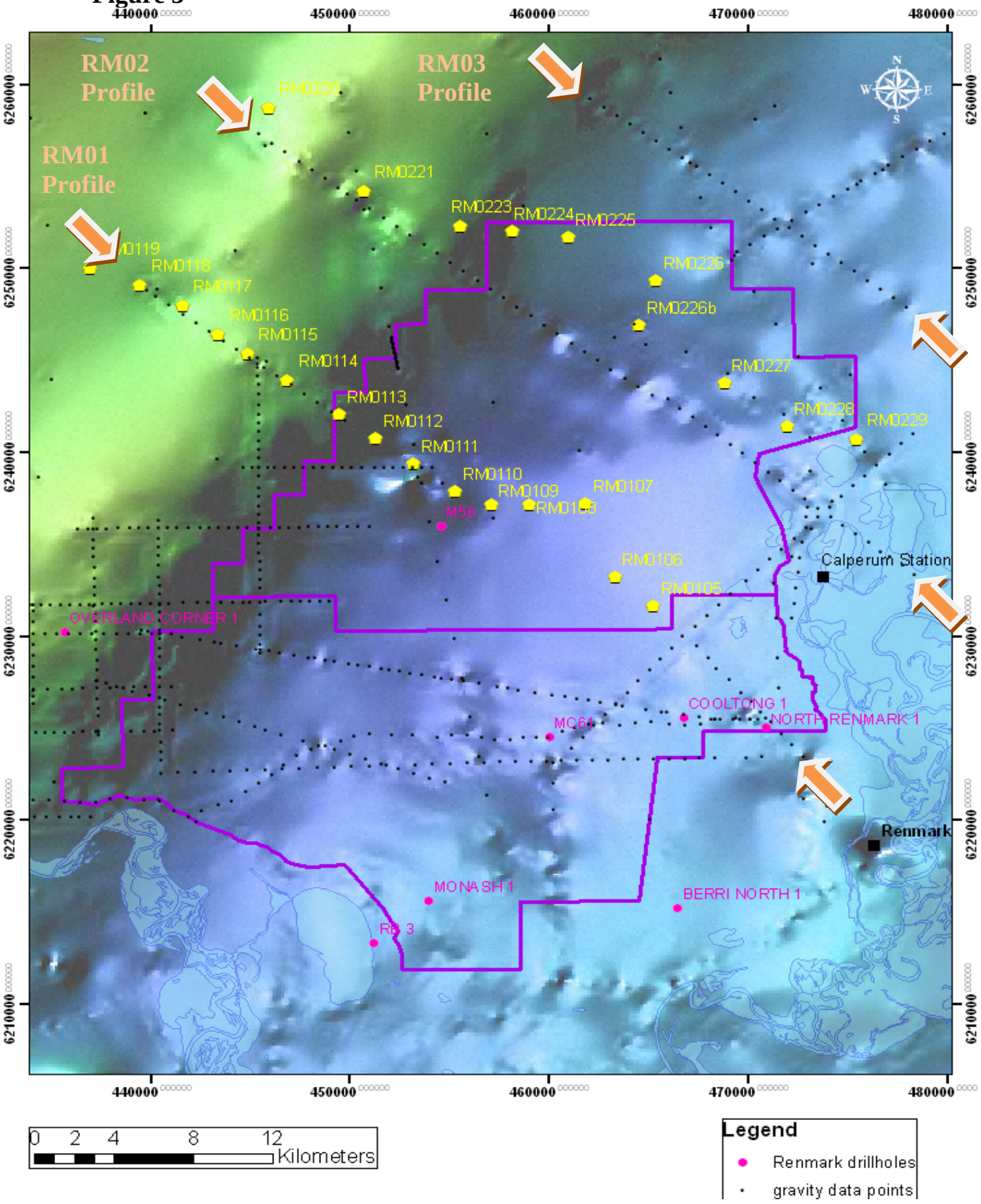
RM02 Profile
RM03 Profile
RM01 Profile
RM0220
RM0221
RM0223
RM0224
RM0225
RM0226
RM0226b
RM0227
RM0228
RM0229
RM0119
RM0118
RM0117
RM0116
RM0115
RM0114
RM0113
RM0112
RM0111
RM0110
RM0109
RM0107
RM0106
RM0105
M56
OVERLAND CORNER 1
Calperum Station
COOLTONG 1
NORTH RENMARK 1
MC64
Renmark
MONASH 1
BERRI NORTH 1
RB 3
440000
450000
460000
470000
480000
6260000
6250000
6240000
6230000
6220000
6210000
N
S
W
E
0 2 4 8 12
Kilometers
Legend
Renmark drillholes
gravity data points

Figure 4

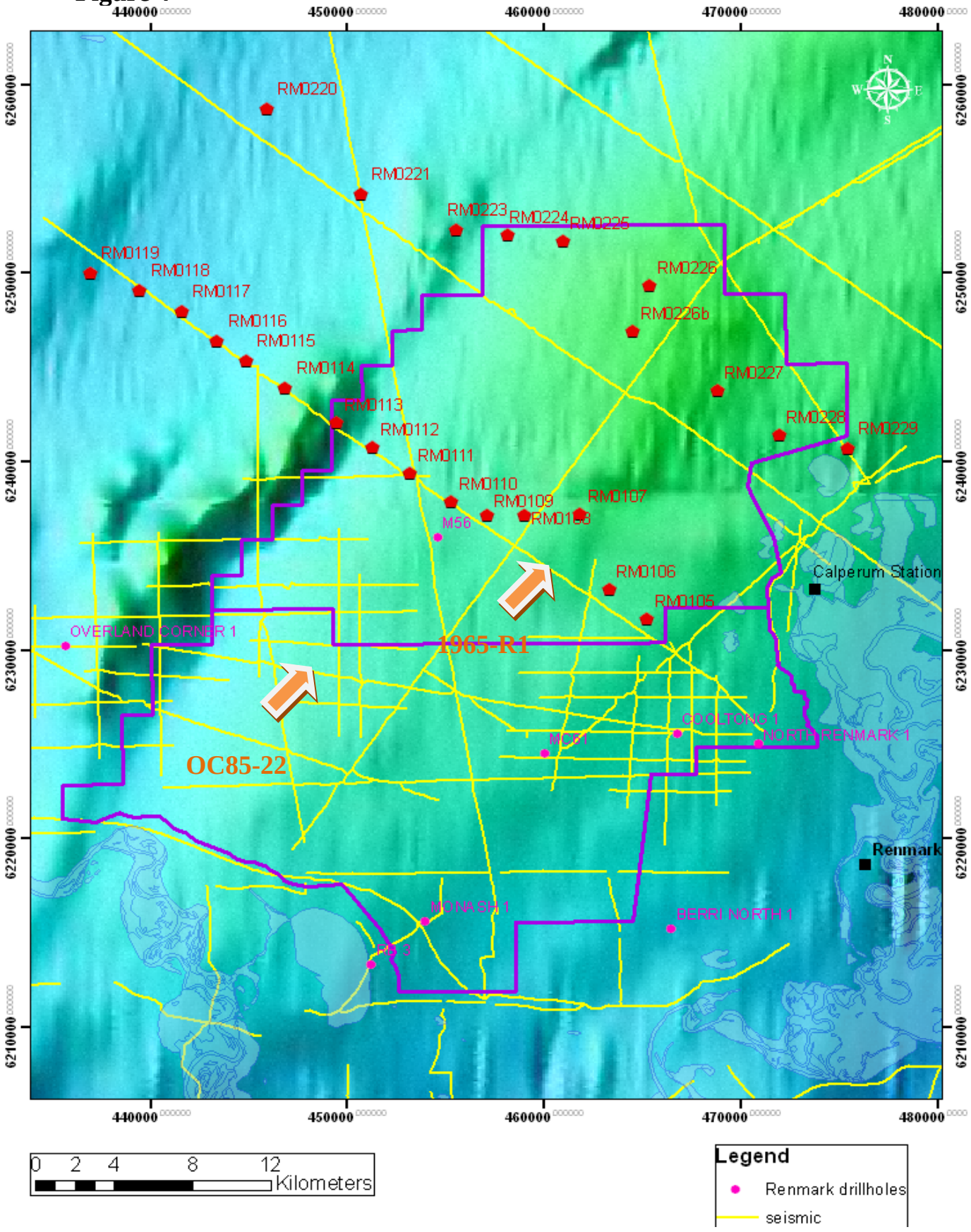
440000
450000
460000
470000
480000
6260000
6250000
6240000
6230000
6220000
6210000
N
W
E
S
RMD220
RMD221
RMD223
RMD224
RMD225
RMD226
RMD226b
RMD227
RMD228
RMD229
RMD119
RMD118
RMD117
RMD116
RMD115
RMD114
RMD113
RMD112
RMD111
RMD110
RMD109
RMD107
RMD106
RMD105
M56
Calperum Station
OVERLAND CORNER 1
1965-R1
OC85-22
GOOLTONG 1
NORTH RENMARK 1
M61
Renmark
MONASH 1
BERRI NORTH 1
0 2 4 8 12
Kilometers
Legend
Renmark drillholes
seismic

Figure 5a

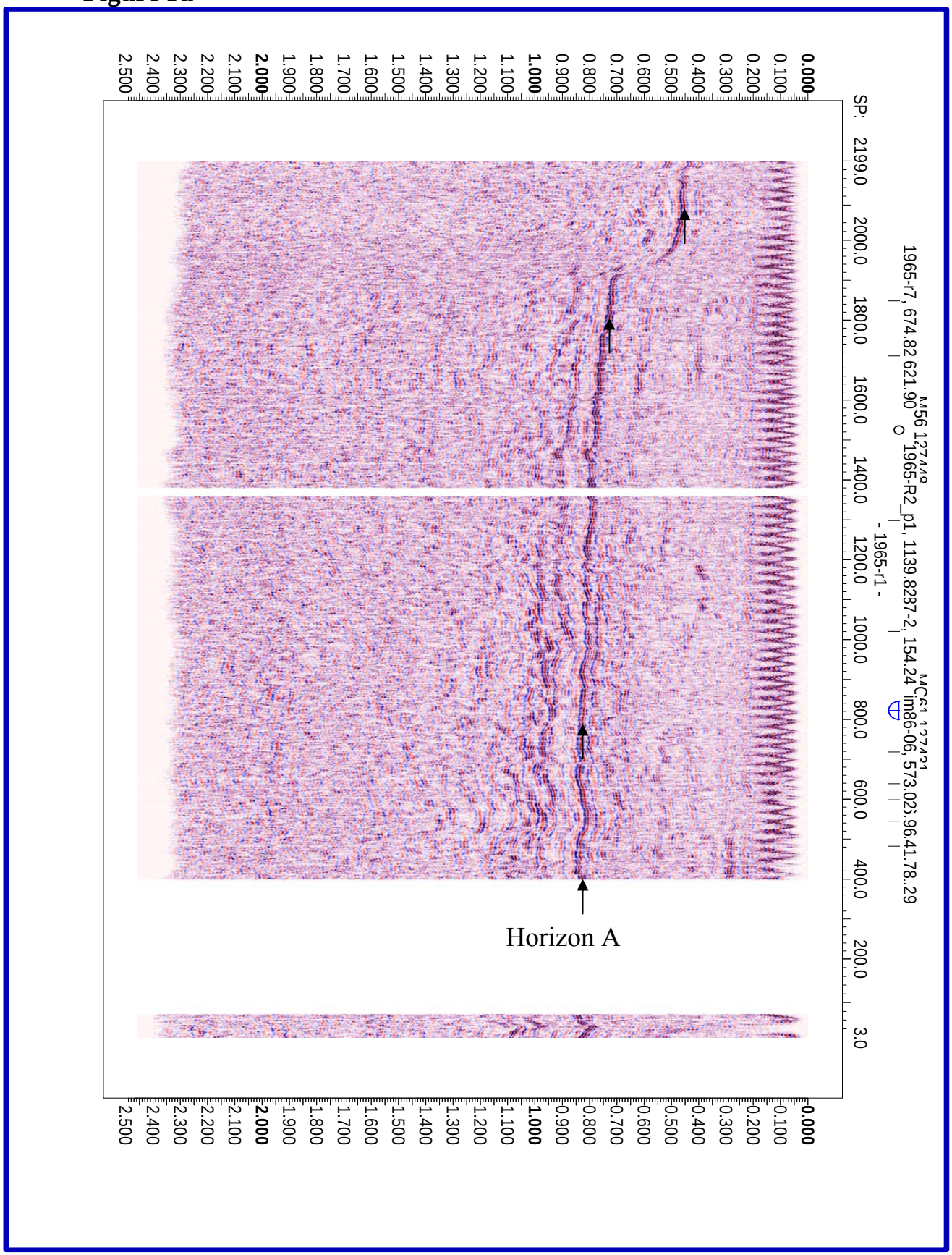
Horizon A
SP:
2199.0
2000.0
1800.0
1600.0
1400.0
1200.0
1000.0
800.0
600.0
400.0
200.0
3.0
0.000
0.100
0.200
0.300
0.400
0.500
0.600
0.700
0.800
0.900
1.000
1.100
1.200
1.300
1.400
1.500
1.600
1.700
1.800
1.900
2.000
2.100
2.200
2.300
2.400
2.500

Figure 5b

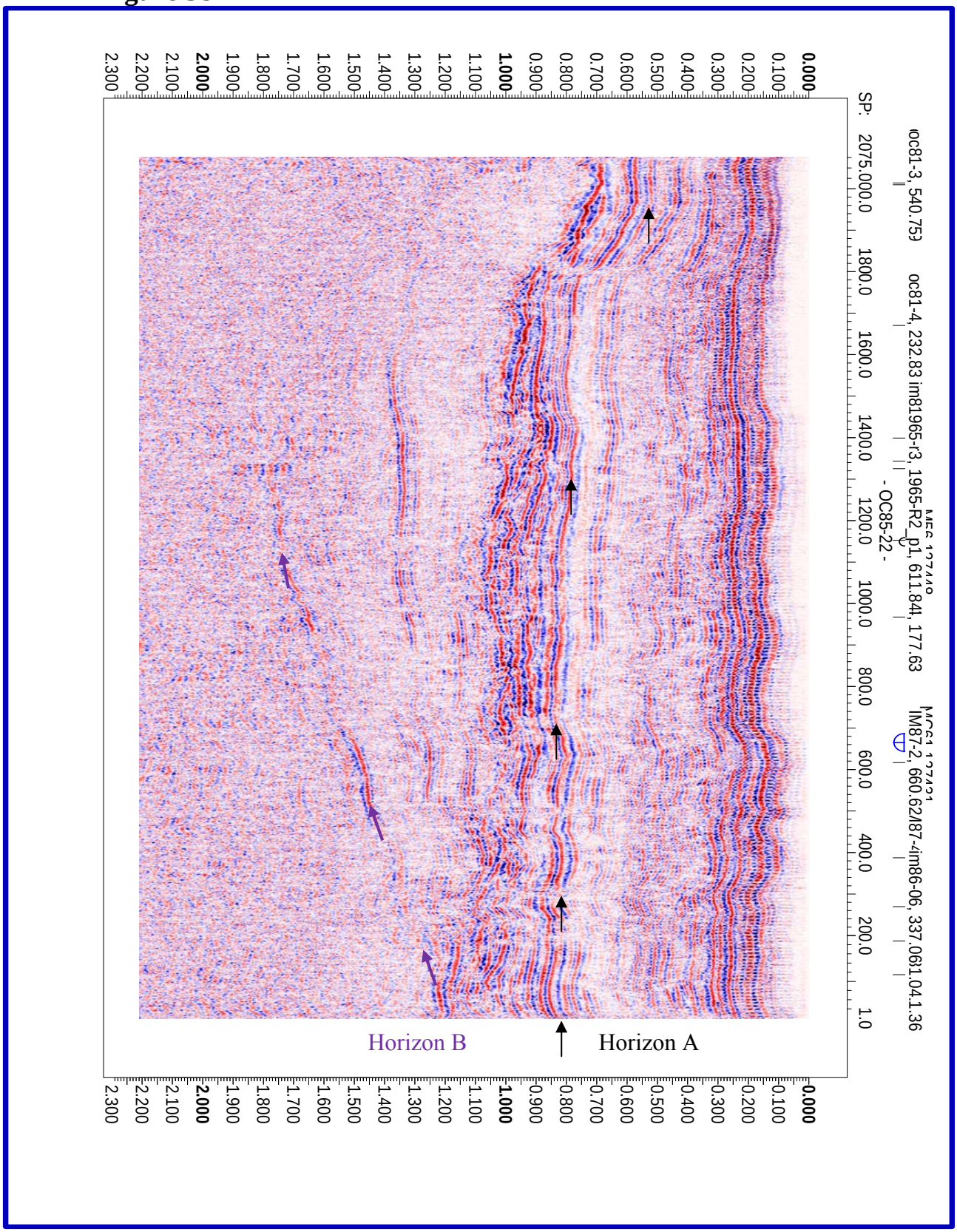

Figure 6a

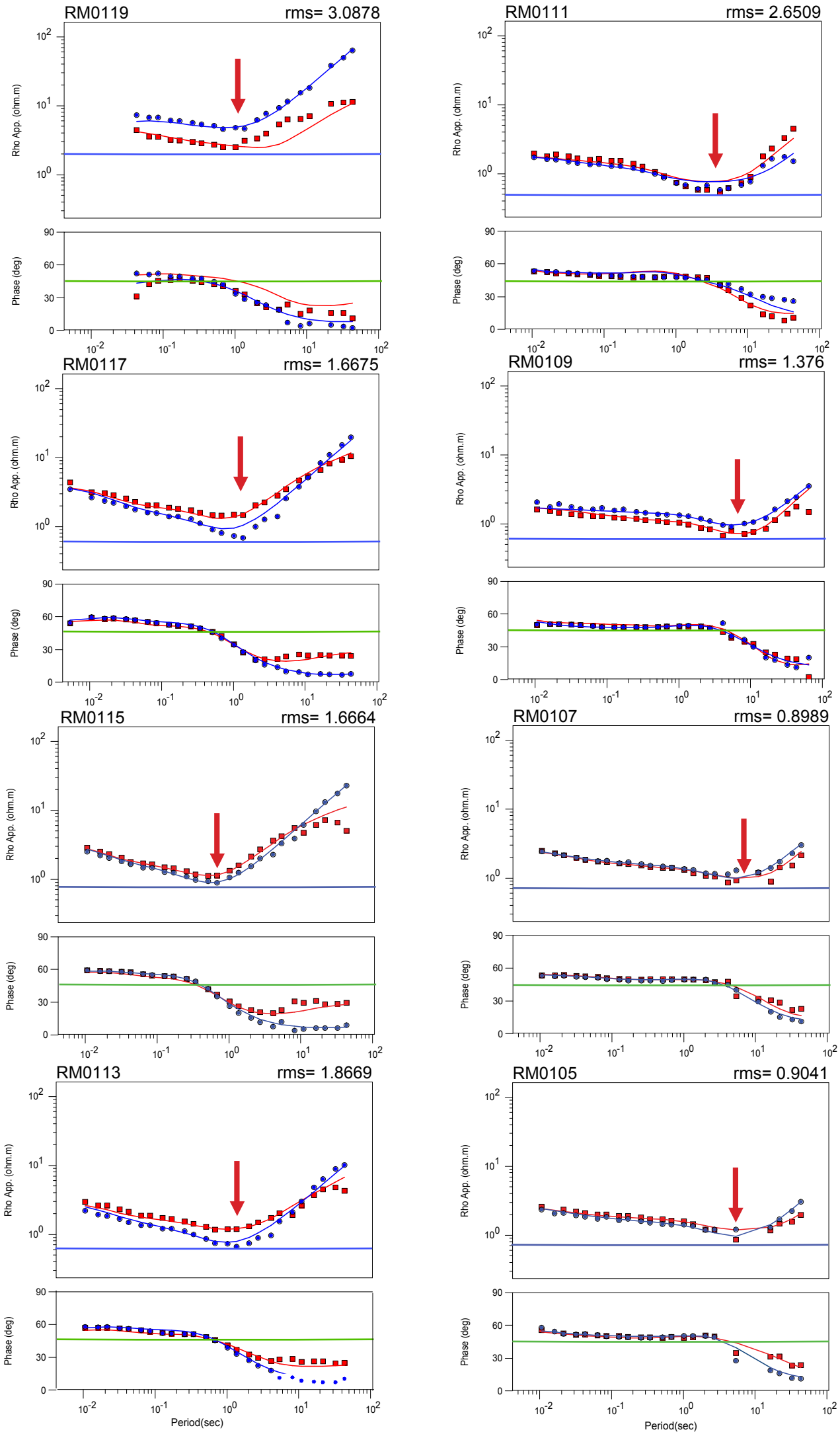
RM0119
rms= 3.0878
RM0111
rms= 2.6509
RM0117
rms= 1.6675
RM0109
rms= 1.376
RM0115
rms= 1.6664
RM0107
rms= 0.8989
RM0113
rms= 1.8669
RM0105
rms= 0.9041
Rho App. (ohm.m)
Phase (deg)
Period(sec)
TM Calculated
TM Original
TE Calculated
TE Original

Figure 6b

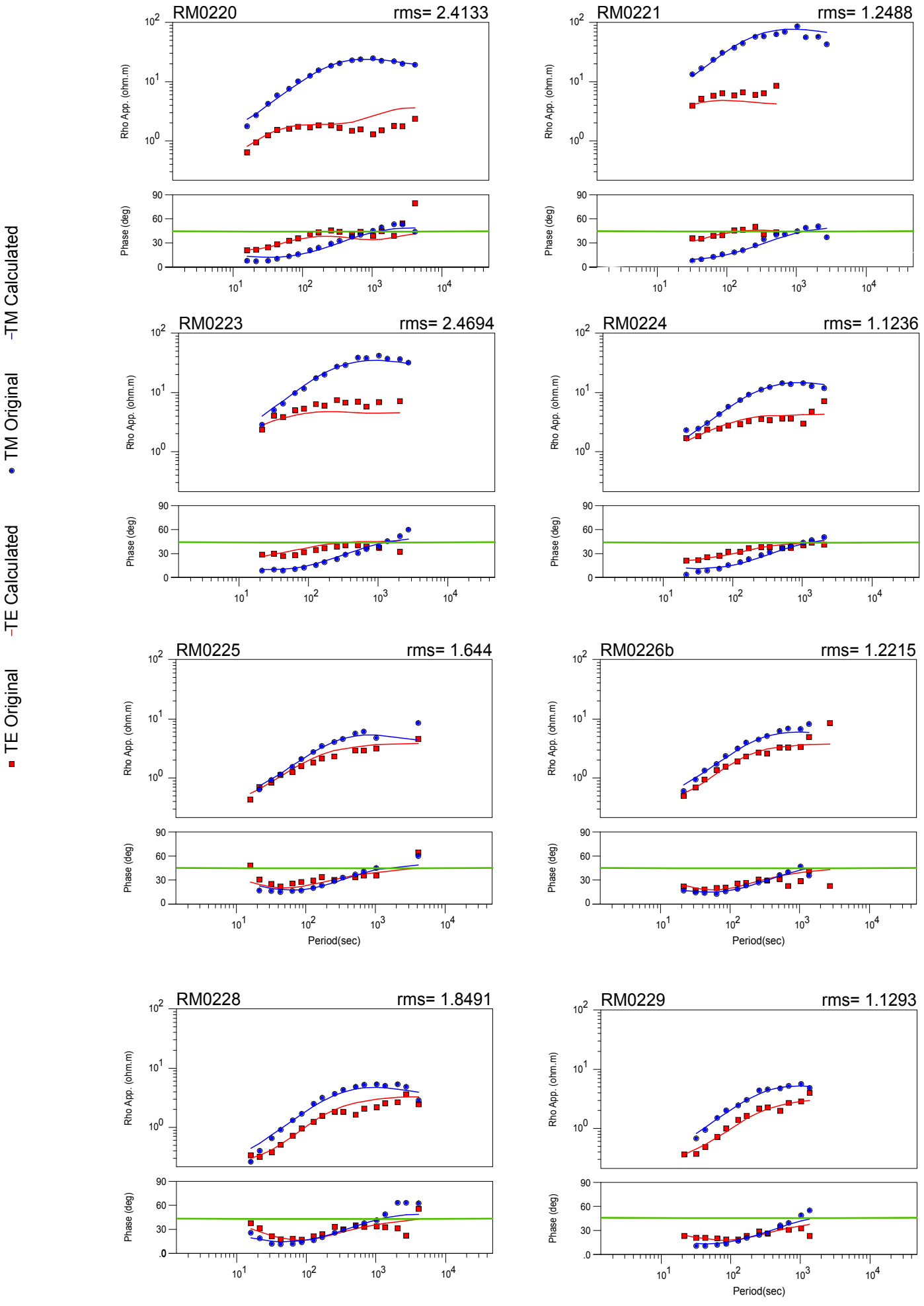
TM Calculated
TM Original
TE Calculated
TE Original
RM0220
rms= 2.4133
RM0221
rms= 1.2488
RM0223
rms= 2.4694
RM0224
rms= 1.1236
RM0225
rms= 1.644
RM0226b
rms= 1.2215
RM0228
rms= 1.8491
RM0229
rms= 1.1293
Rho App. (ohm.m)
Phase (deg)
Period(sec)

Figure 7

a) RM01 Unconstrained MT Model

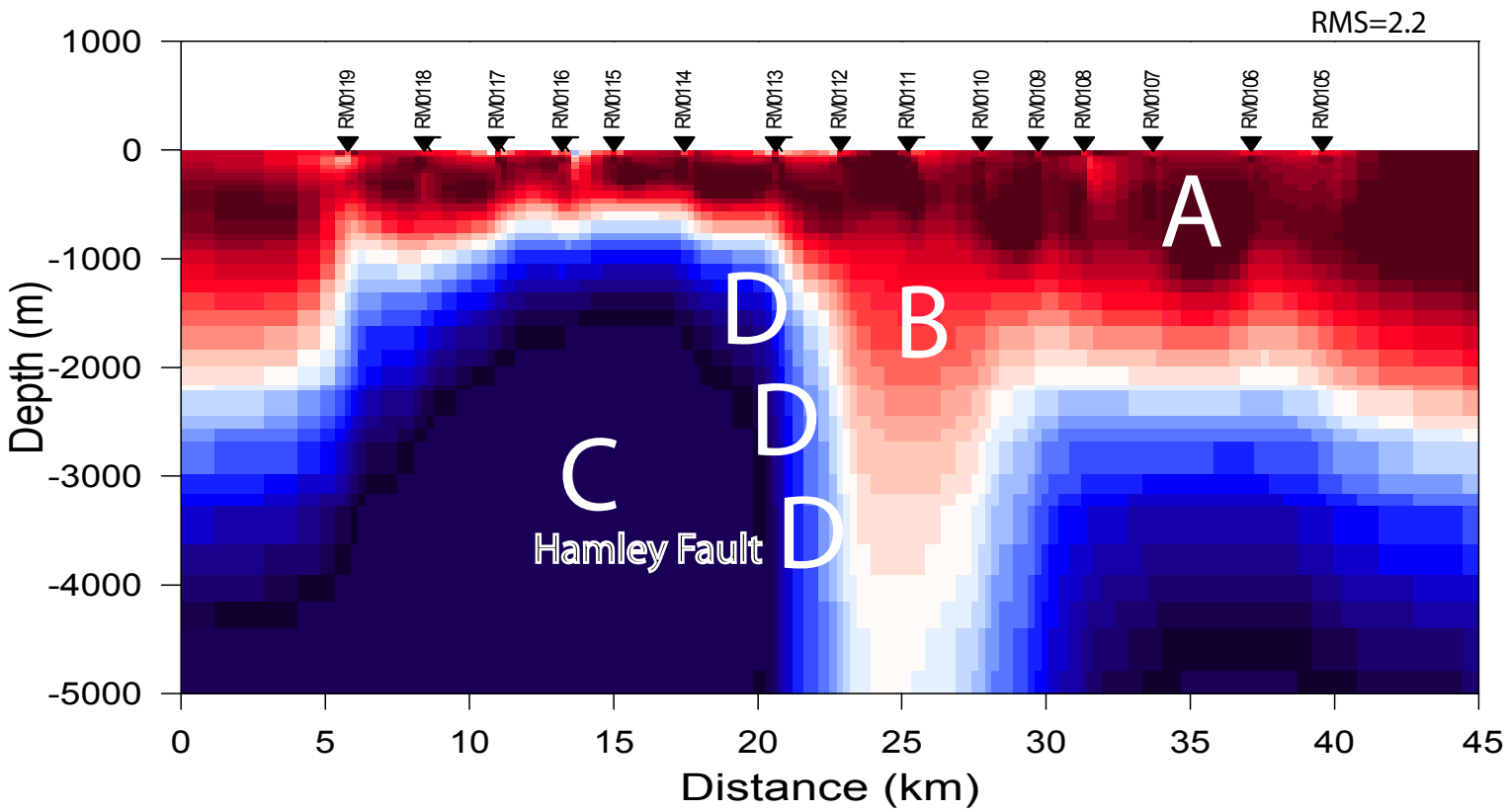

b)RM02 MT Model

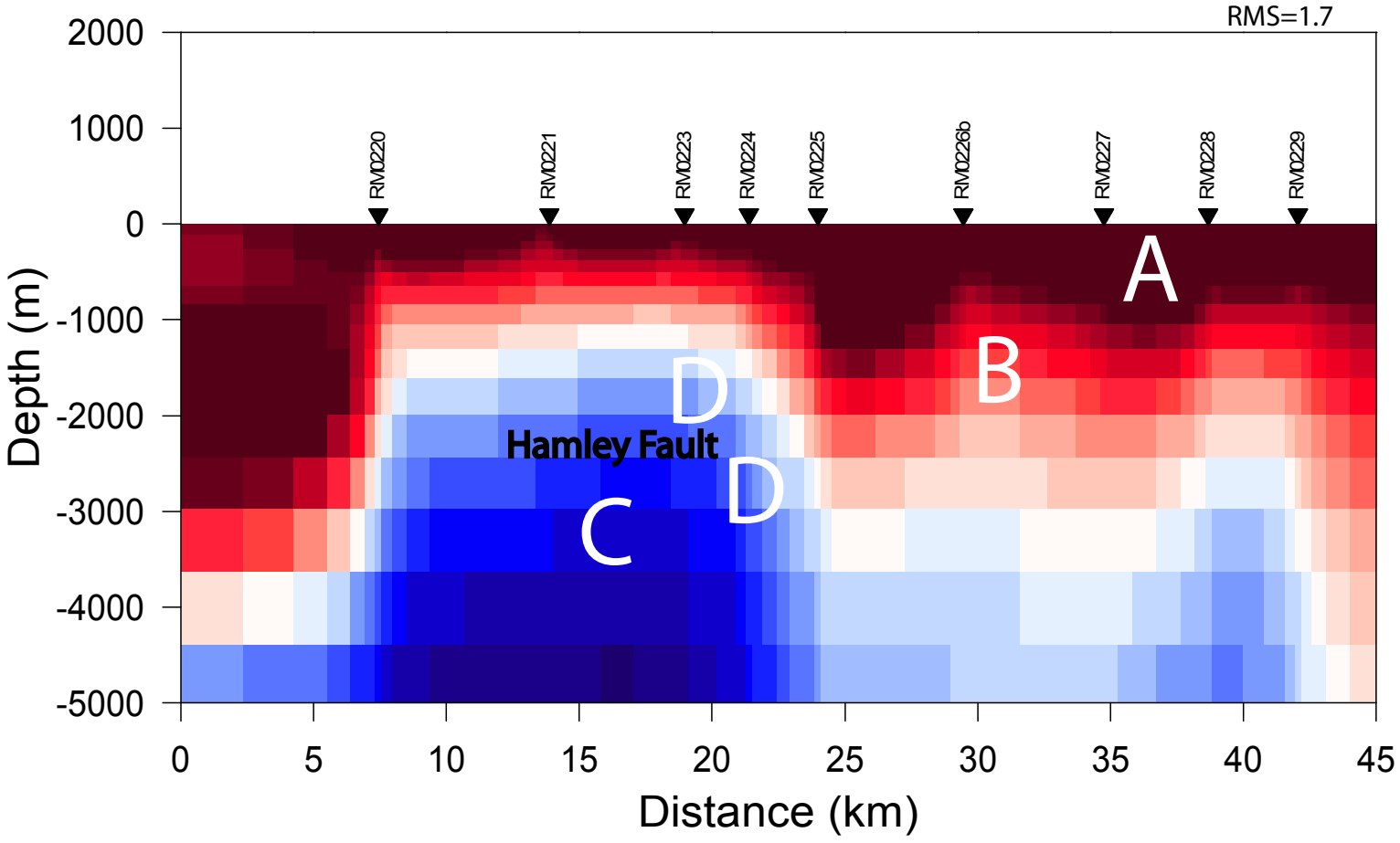

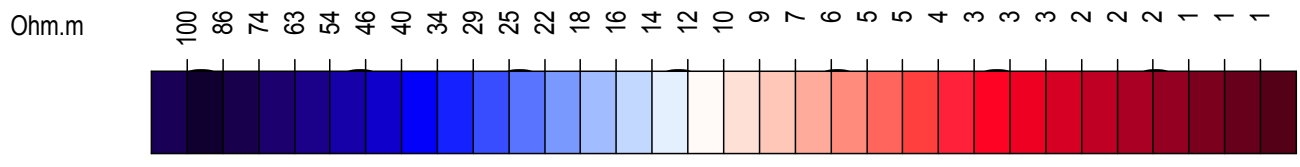

Figure 8

a) Line 1965-R1

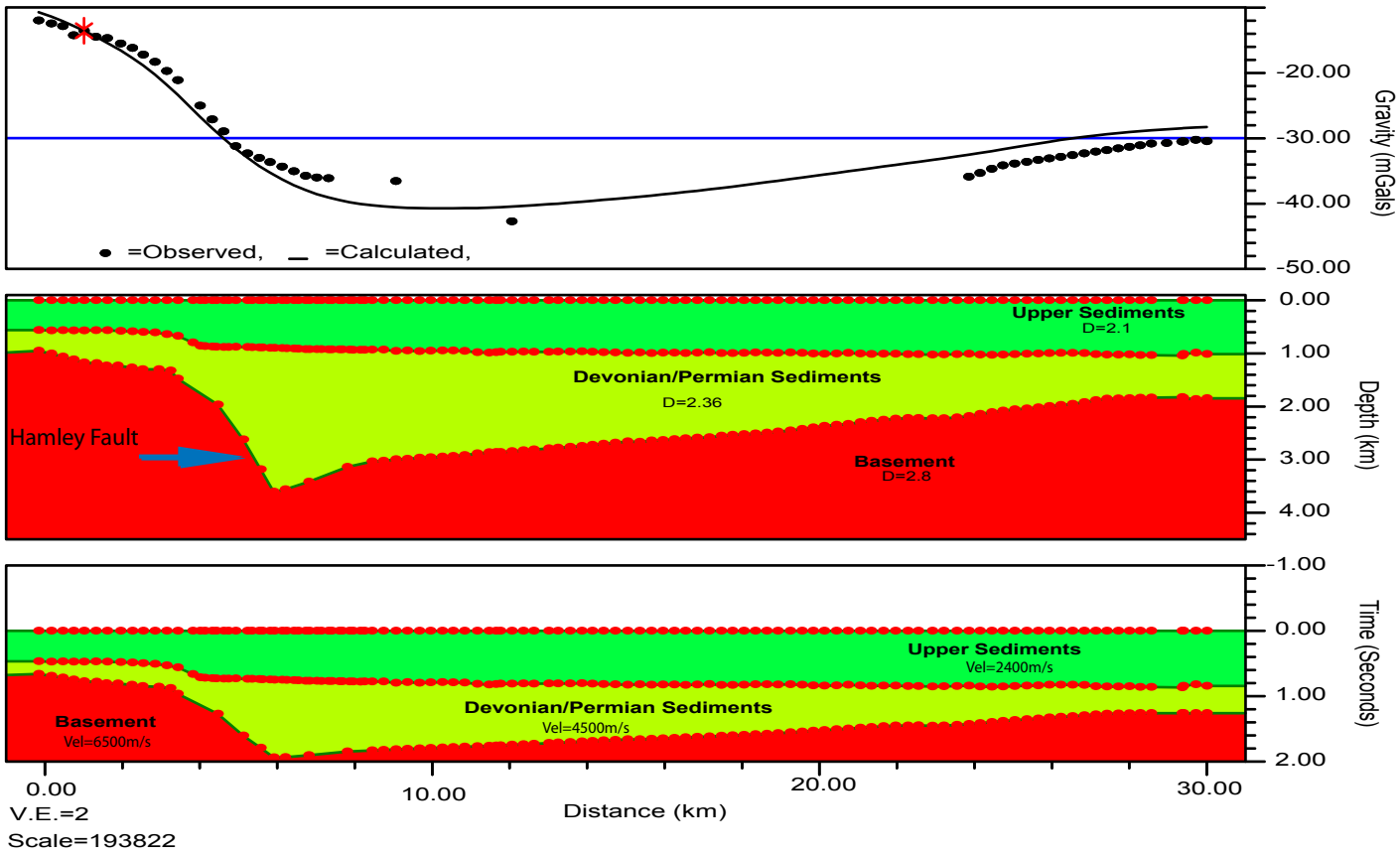

b) Line OC85-22

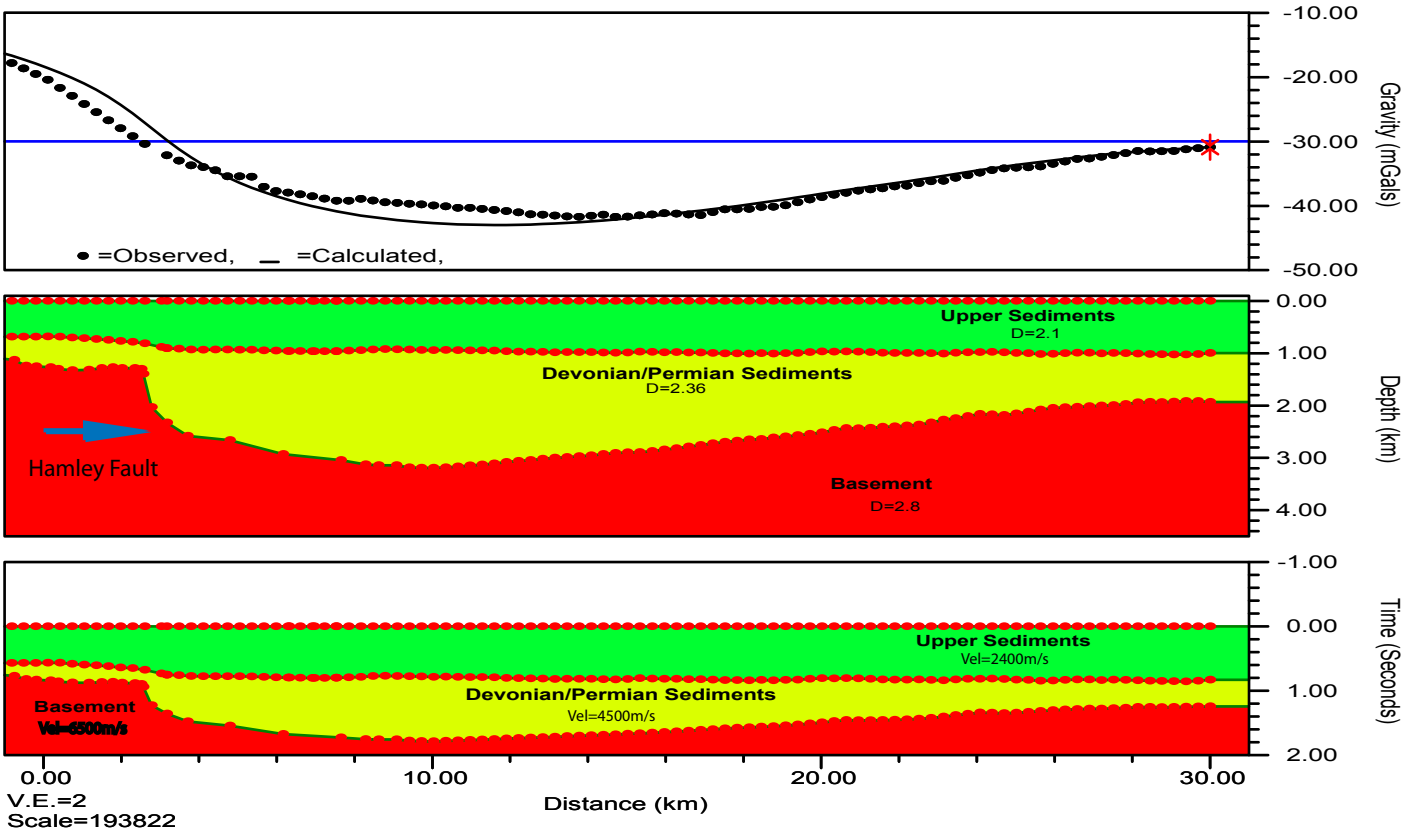

Figure 9

a) RM03

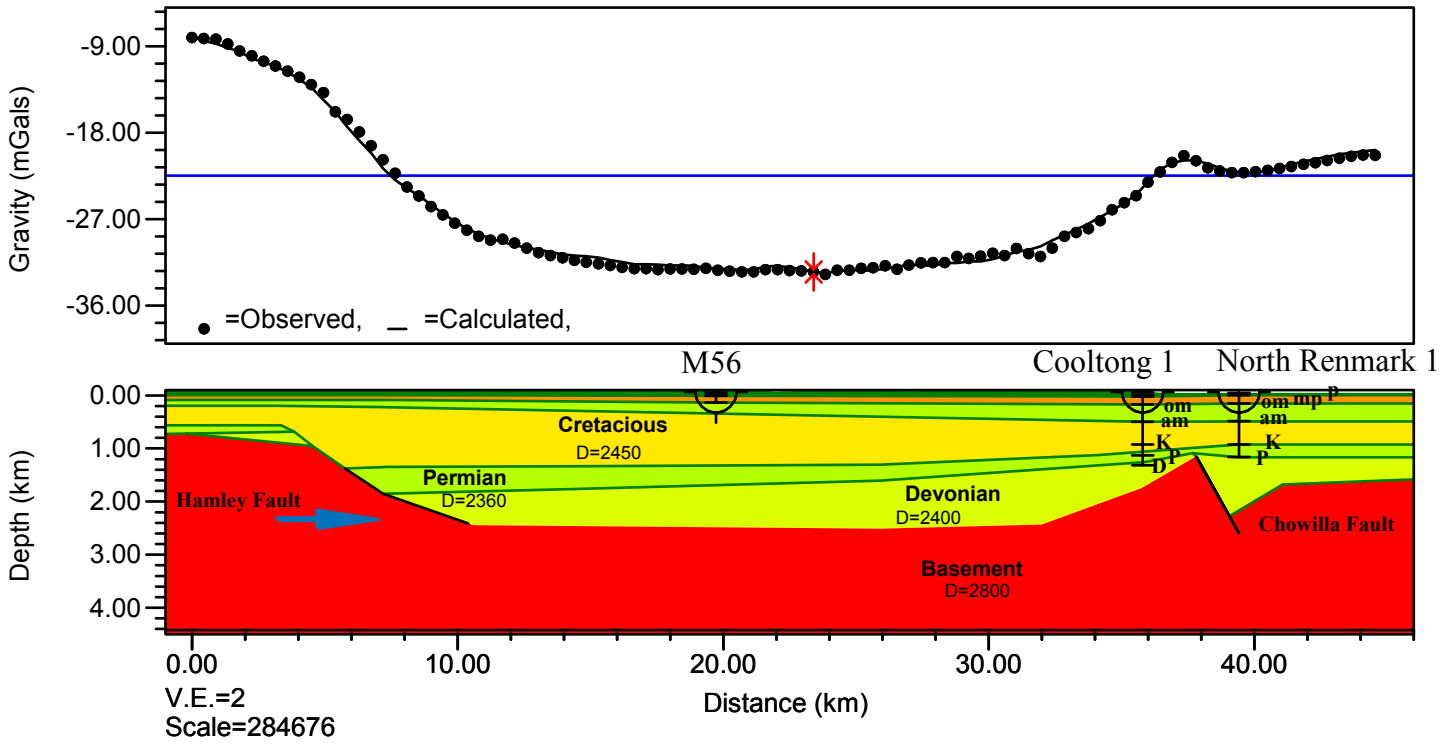

b) RM02

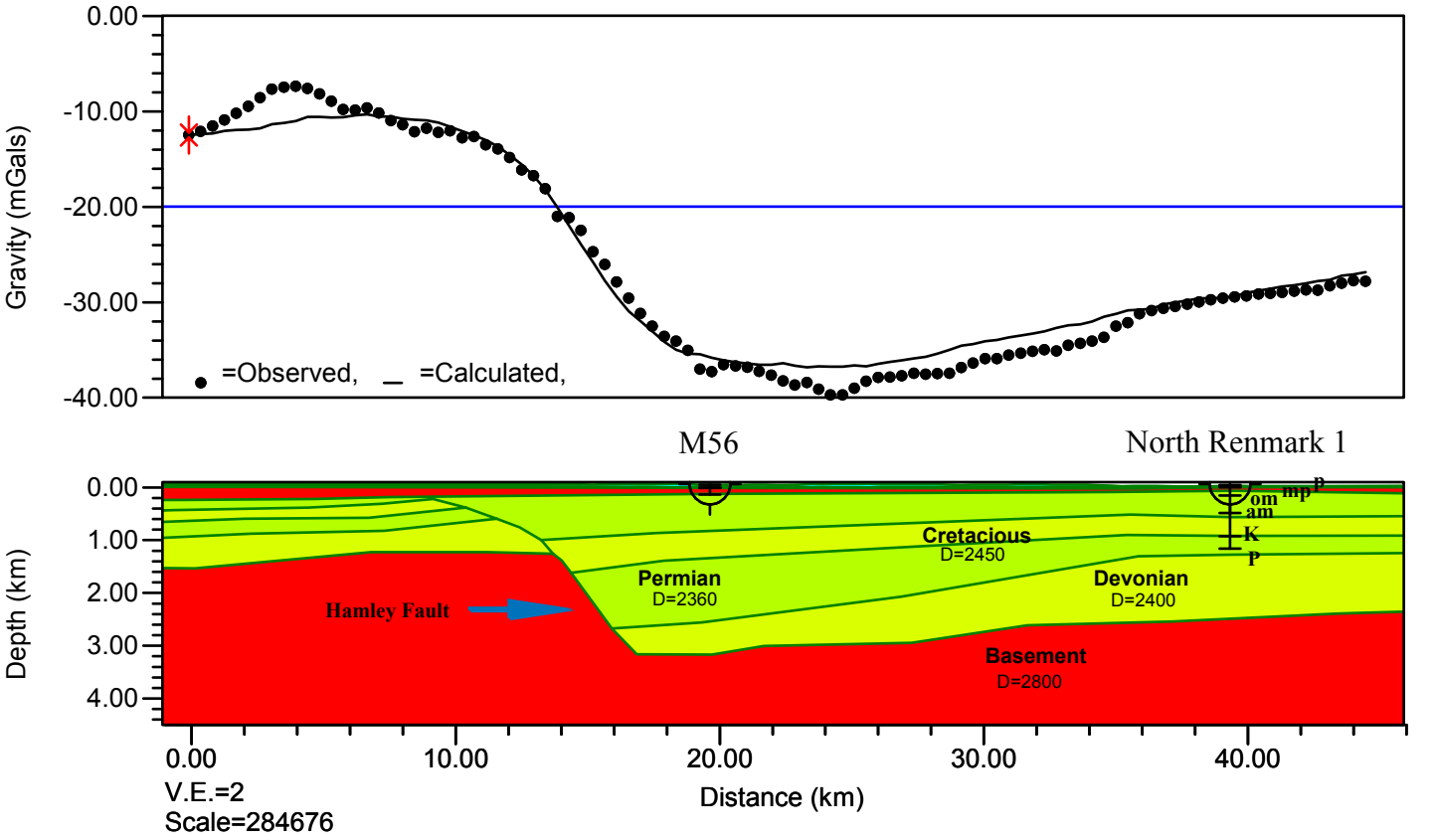

Figure 10

a) RM01 Unconstrained MT Model

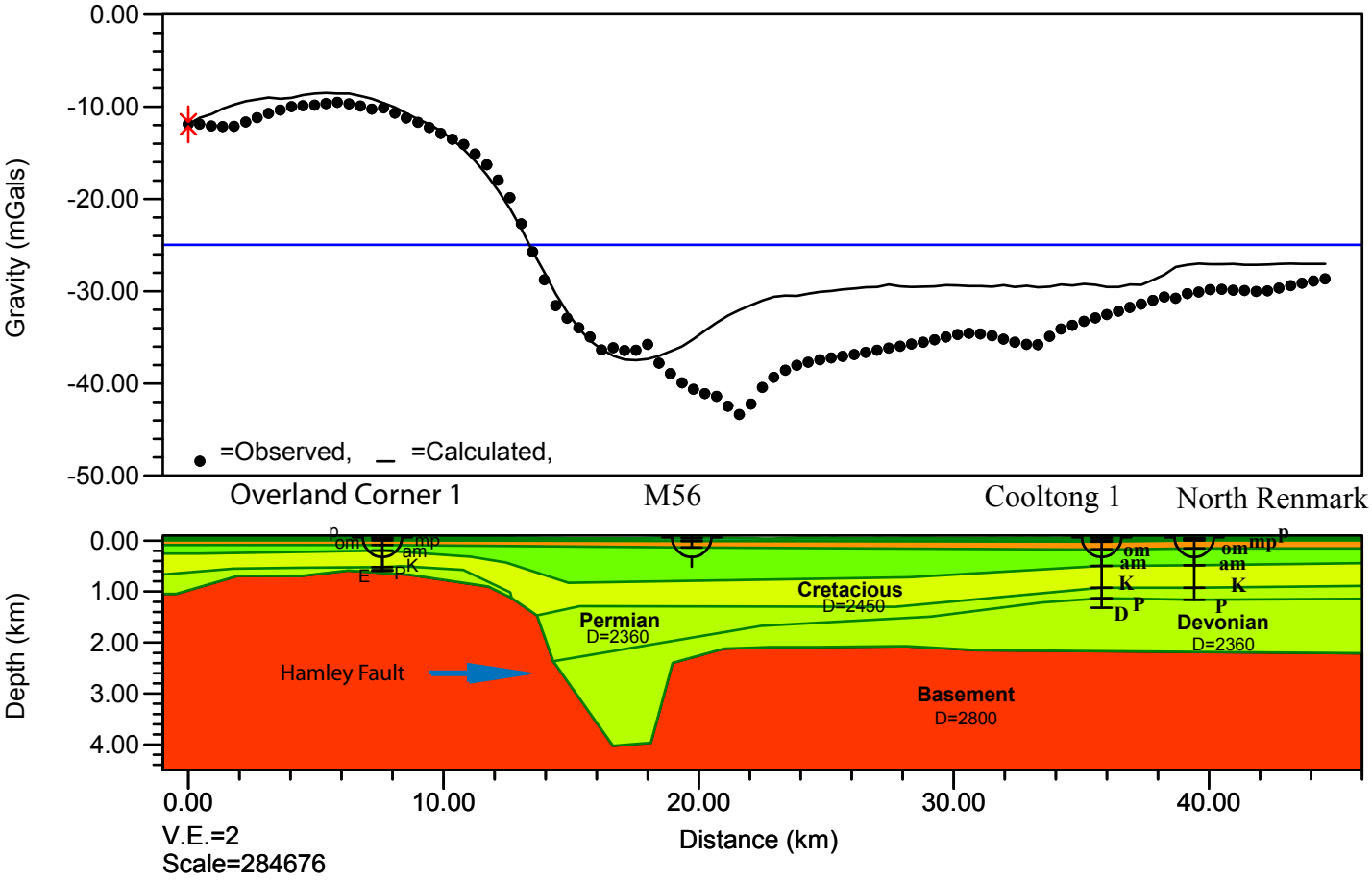

b) RM01 Seismic Constrained MT Model

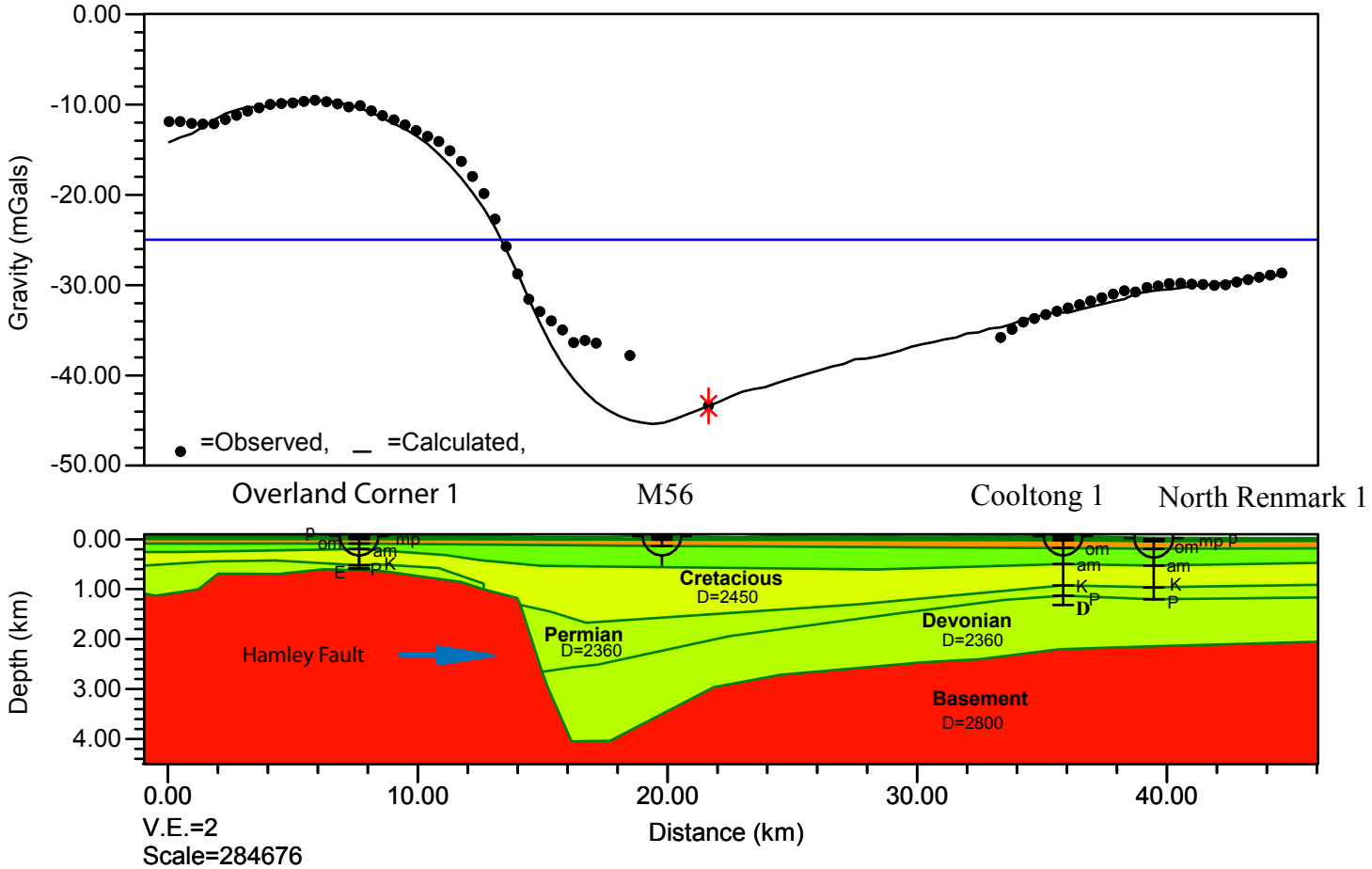

Figure 11

a)

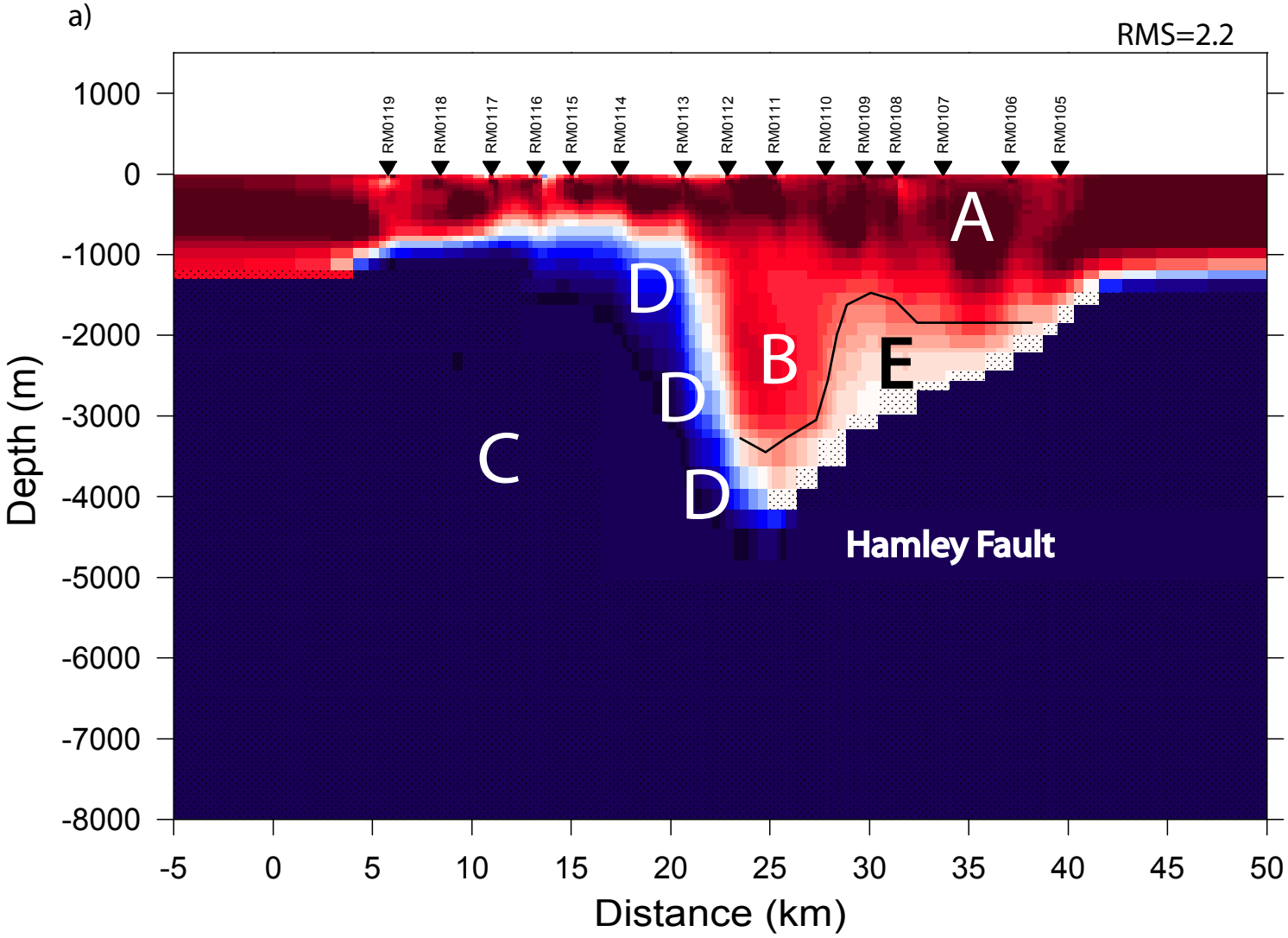
RMS=2.2
RM0119
RM0118
RM0117
RM0116
RM0115
RM0114
RM0113
RM0112
RM0111
RM0110
RM0109
RM0108
RM0107
RM0106
RM0105
A
B
C
D
D
D
E
Hamley Fault
Depth (m)
1000
0
-1000
-2000
-3000
-4000
-5000
-6000
-7000
-8000
-5
0
5
10
15
20
25
30
35
40
45
50
Distance (km)

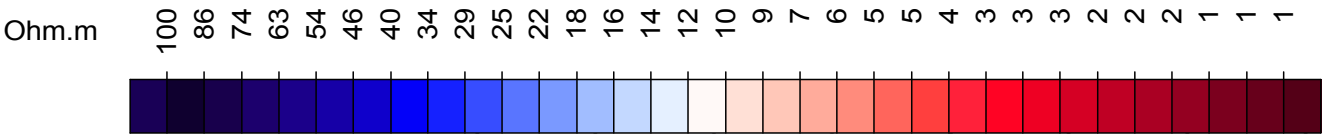
Ohm.m
100
86
74
63
54
46
40
34
29
25
22
18
16
14
12
10
9
7
6
5
5
4
3
3
3
2
2
2
1
1
1

b)

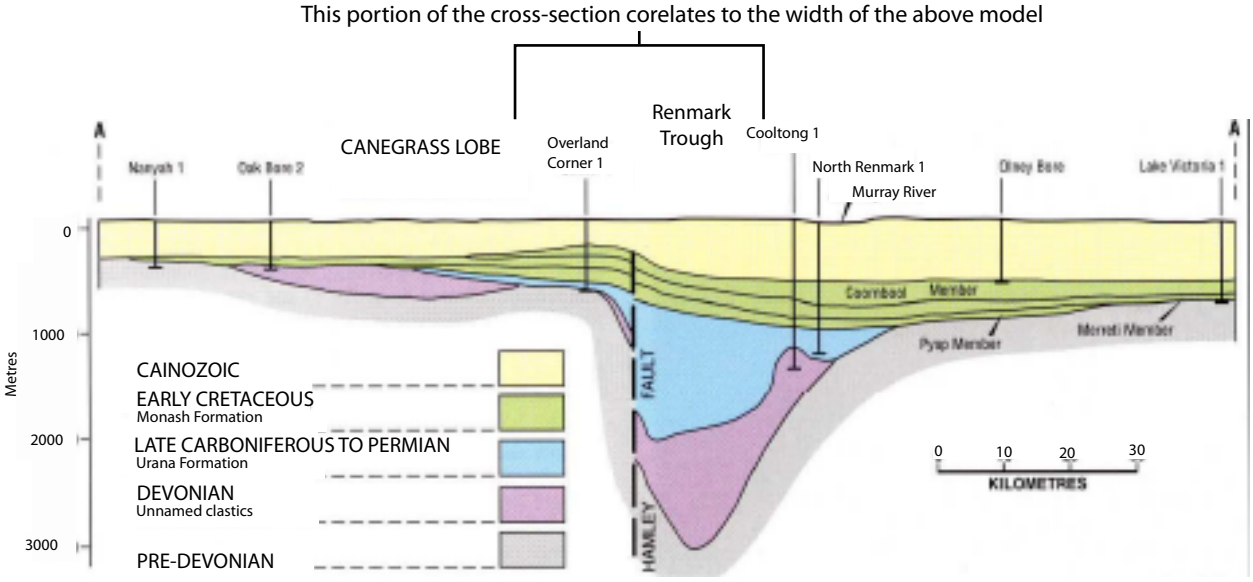
This portion of the cross-section corelates to the width of the above model
A
CANEGRASS LOBE
Overland Corner 1
Renmark Trough
Cooltong 1
North Renmark 1
Murray River
A
0
1000
2000
3000
Metres
CAINOZOIC
EARLY CRETACEOUS
Monash Formation
LATE CARBONIFEROUS TO PERMIAN
Urana Formation
DEVONIAN
Unnamed clastics
PRE-DEVONIAN
FAULT
HAMLEY
Pyap Member
0
10
20
30
KILOMETRES

Figure 12a

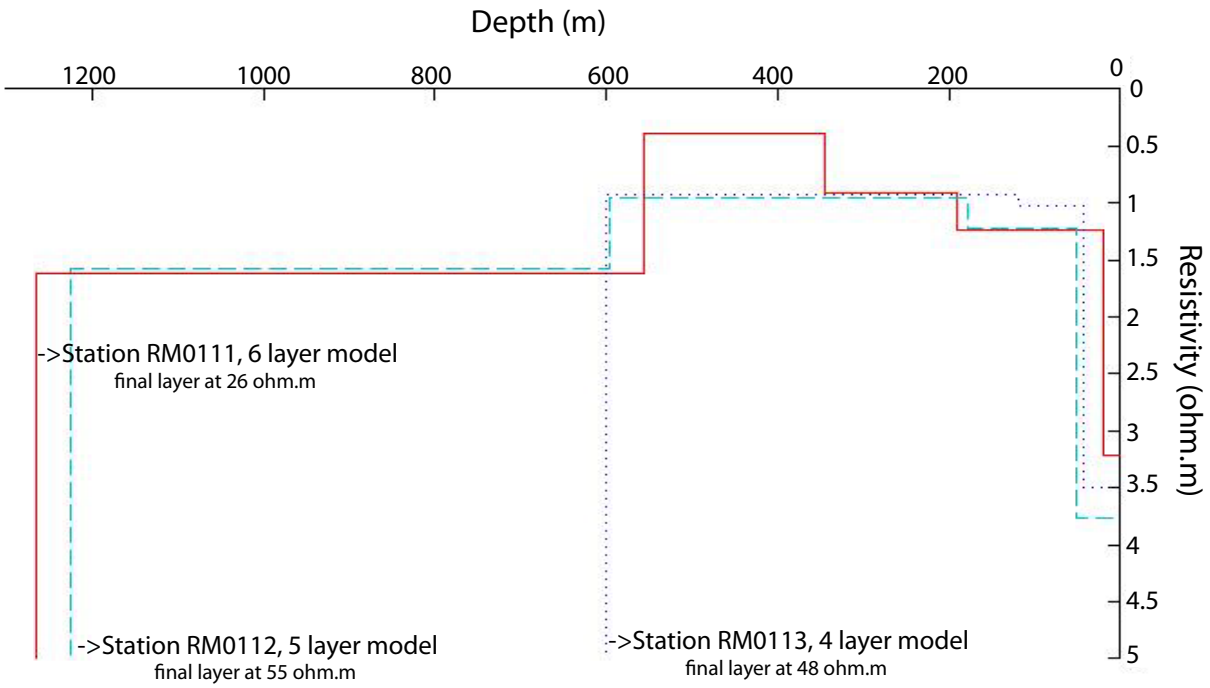

Cooltong 1 Lithology

Depth to bottom of package (m)	Package	Description
4	ns	Ground surface
58	p	Sandstone, medium-coarse grained
82	mp	Sandstone, very coarse, interbedded claystone
236	om	Limestone, texture changes from
		crystalline-dolomitic-clayey
558	am	Sandstone, fine-coarse grained, interbedded claystone
984	K	Siltstone with interbedded clay and sandstone
1189	P	Shale with interbedded sandstone
1380	D	Interbedded sandstone, fine-coarse grained and
		interbedded siltstone/claystone

North Renmark 1 Lithology

Depth to bottom of package (m)	Package	Description
18	ih	Unconsolidated clay and sand
43	p	Sandstone, coarse grained, clayey in part with minor
		siltstone
61	mp	Siltstone
215	om	Limestone/marl grading into siltstone/marl
549	am	Mudstone and siltstone interbedded with fine-medium
		grained sandstone
989	K	Shale/siltstone - sandstone/siltstone
1225	P	Interbedded siltstone and shale

Sand: $por = 0.617 * e^{(-5.55e-4 * depth)}$ shale: $por = 0.630 * e^{(-5.71e-4 * depth)}$ silt: $por = 0.803 * e^{(-7.95e-4 * depth)}$

Constants a=0.88 and m=1.32 generally tertiary

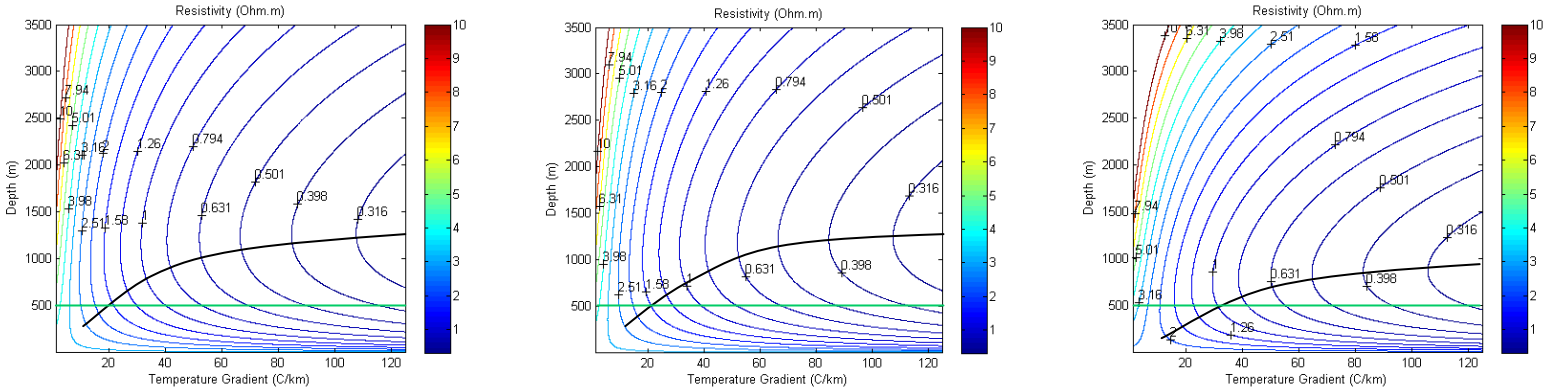

Constants a=0.62 and m=1.72 generally Mesozoic

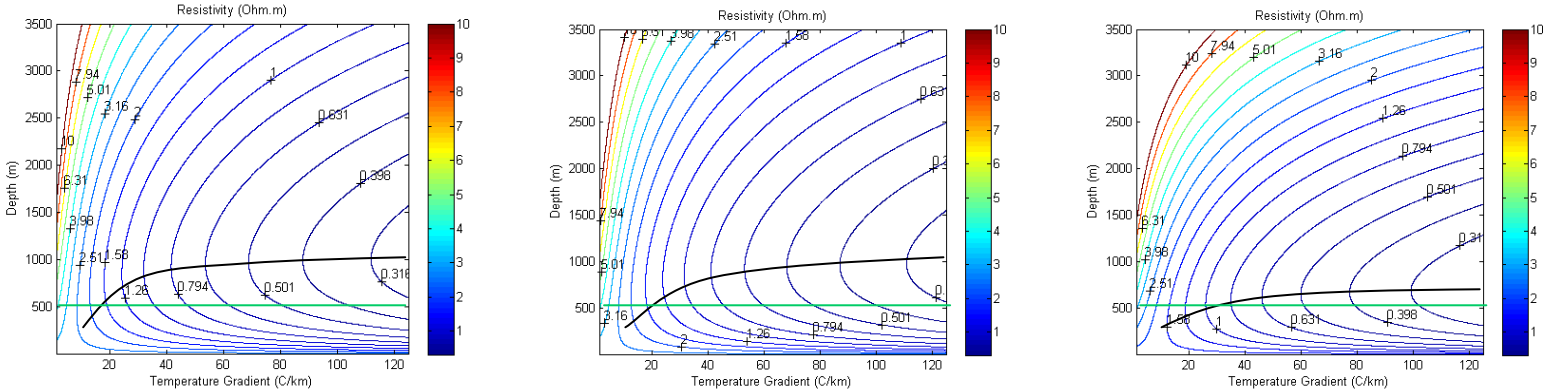

Constants a=0.62 and m=1.95 generally paleozoic

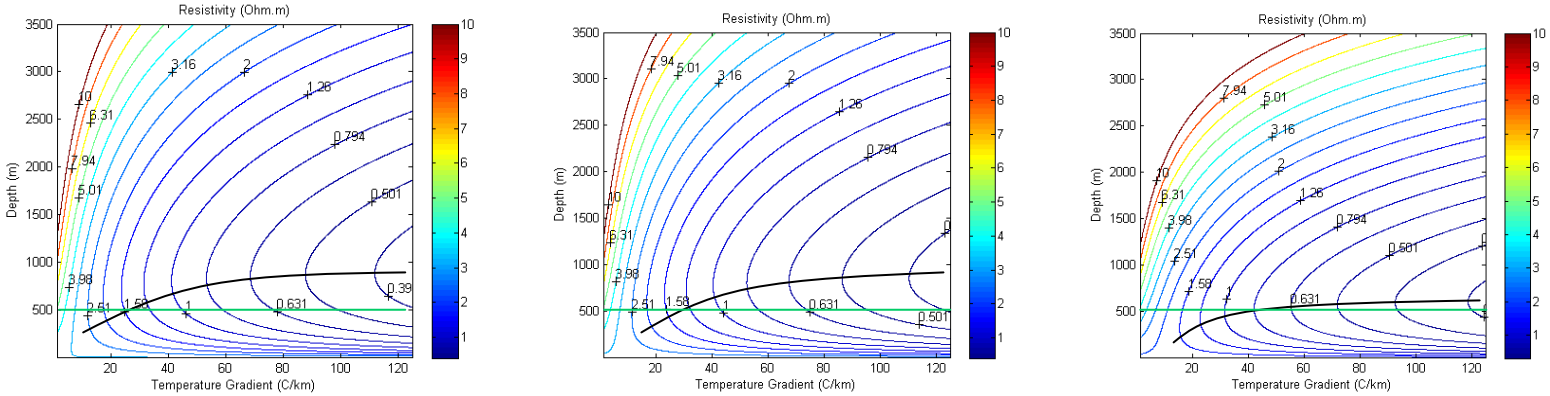

Figure 12b

Constants a=0.88 and m=1.32 changing values of compaction constant for sand.

$por = 0.617 * e^{(-5.55e-4 * depth)}$

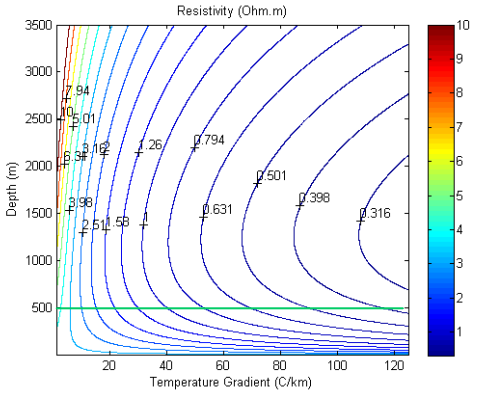

$por = 0.617 * e^{(-9.99e-4 * depth)}$

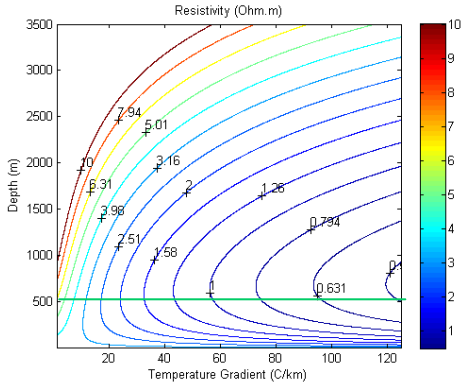

$por = 0.617 * e^{(-12.99e-4 * depth)}$

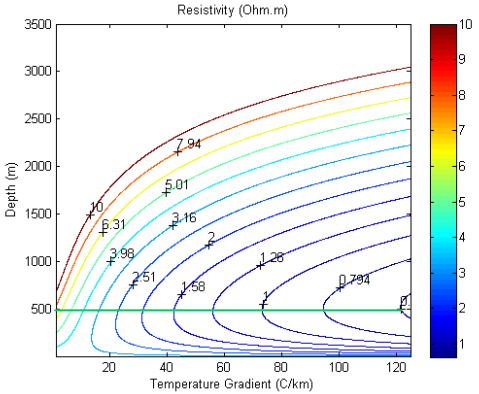

$por = 0.617 * e^{(-14.99e-4 * depth)}$

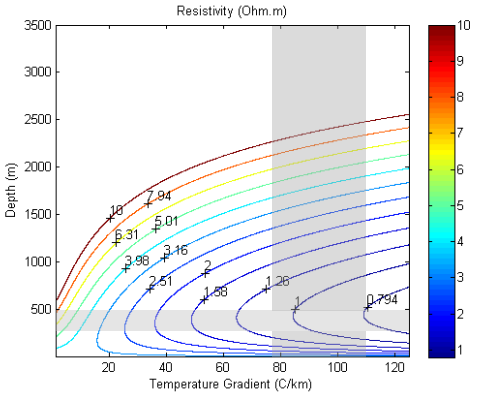

Constants a=0.88 and m=1.32 changing values of compaction constant for silt.

$por = 0.803 * e^{(-7.95e-4 * depth)}$

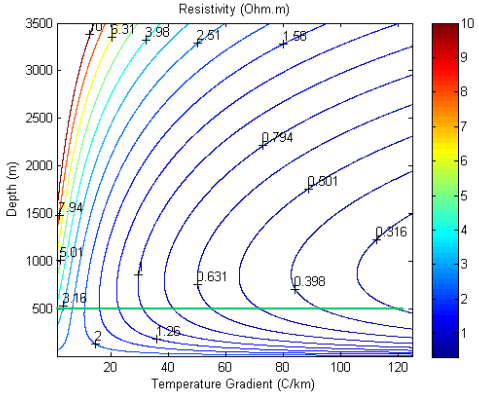

$por = 0.803 * e^{(-9.95e-4 * depth)}$

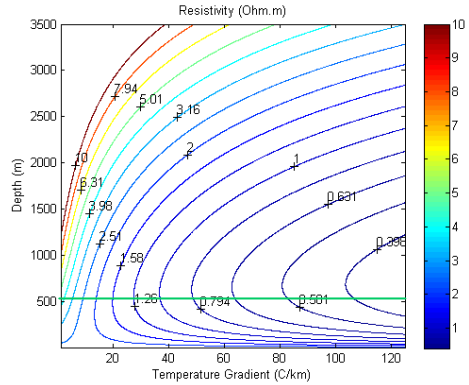

$por = 0.803 * e^{(-12.95e-4 * depth)}$

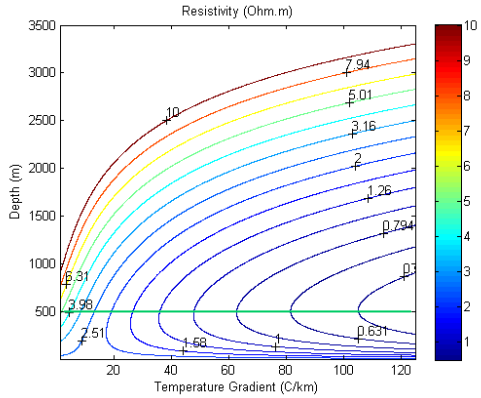

$por = 0.803 * e^{(-14.95e-4 * depth)}$

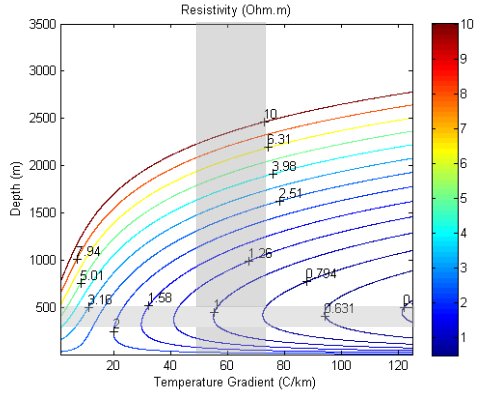

Figure 12c